# Dynamic Light Scattering Analysis in Biomedical Research and Applications of Nanoparticles and Polymers

Alexander Knysh, Pavel Sokolov, Igor Nabiev

# Dynamic Light Scattering Analysis in Biomedical Research and Applications of Nanoparticles and Polymers

**Alexander Knysh[1]*, Pavel Sokolov[1], and Igor Nabiev[1,2+]**

[1] National Research Nuclear University MEPhI (Moscow Engineering Physics Institute), 31 Kashirskoe shosse, Moscow 115409, Russian Federation

[2] Université de Reims Champagne-Ardenne, 51 rue Cognacq Jay, Reims 51100, France

**e-mail:** *knyshkikai@mail.ru,+igor.nabiev@gmail.com

**Abstract.** Dynamic light scattering (DLS) is one of the most commonly used photonic methods for estimating the hydrodynamic radius, ζ-potential, polydispersity, and concentrations of nanoparticles (NPs), polymers, and cells, as well as for studying changes in these parameters upon interaction or aggregation of molecules and particles. NPs and polymers are components of numerous drugs, cosmetics, and food industry products. Hence, the monitoring of their physical, chemical, and morphological properties, often related to their functional characteristics and toxicity, are of vital importance. This review deals with the specifics of the DLS method as applied to the analysis of samples of different types and the modifications of this method depending on the characteristics of the samples. The theoretical basis of the DLS method and its applications to the study of NPs, polymers, and their interactions are presented, with the focus on biomedical applications. The last section of the review considers the advantages and limitations of DLS analysis as compared with other photonic analytical methods, as well as future trends in the development of this approach. © 2023 Journal of Biomedical Photonics & Engineering.

**Keywords:** dynamic light scattering; nanoparticles; polymers; hybrid materials; ζ-potential; hydrodynamic diameter.

Paper #8681 received 2 Mar 2023; revised manuscript received 13 Apr 2023; accepted for publication 17 Apr 2023; published online 30 May 2023. doi: 10.18287/JBPE23.09.020203.

## 1 Introduction

Photonic methods of analysis based on various principles of light–matter interaction are widely used to analyze both organic (including biological) and inorganic objects. Light can be absorbed, refracted, or reflected upon its interaction with molecules, or change its plane of polarization or wavelength. These effects have been employed in a variety of methods of analysis in medicine, biology, biosensing, detection and analysis of mineral resources, and many other fields of science and technology. For example, Raman spectroscopy is used to study chemical bonds, to identify molecules, and to study their structure, which allows the detection of various microorganisms [1] or to use this approach in the diagnosis of cancer [2] and many other diseases. Specific light absorption by protein molecules at 280 nm, and the maximum absorption of radiation by nucleotides at 260 nm are used to determine the concentrations of proteins and nucleic acids, respectively [3, 4]. Estimation of light polarization and measurement of circular dichroism spectra can be used to study the chirality of compounds, such as amino acids, monosaccharides, or drugs [5, 6]. In refractometry, the measurement of the refractive index is used to determine the concentrations of chemical compounds in solutions [7], which is used in cell biology, hematology [8], and other fields. Thus, optical methods make it possible to study the composition and structure of biological objects at the atomic and molecular levels. These optical methods are also successfully used for identifying organic molecules and determining the concentration and purity of biopolymers.

Unlike the approaches mentioned above, the dynamic light scattering (DLS) method is suitable for estimating macroscopic parameters of objects, such as the size of

nanoparticles (NPs), microparticles, and polymers and the ζ-potential of their surface, as well as for studying the interaction of polymers, cells, NPs, and microparticles of various types. It is especially important that DLS can be used to study biological polymers in liquid phase, in their natural environment, whereas many other methods of determining macroscopic parameters, such as electron and atomic force microscopies, require the sample to be transferred to the dry or partly dehydrated phase.

Liposomes, polymers, and NPs of various compositions are examples of advanced drug delivery systems that have proved to be promising in delivering drugs effectively and selectively to target cells or tissues. Liposomes are spherical vesicles composed of a phospholipid bilayer that can encapsulate both hydrophilic and hydrophobic drugs. These vesicles can be made in different sizes and can be functionalized with specific ligands to target specific cells or tissues. The use of liposomes as a drug delivery system has several advantages, including improved drug solubility, increased drug stability, prolonged drug circulation time, and reduced toxicity [9]. Several liposomal formulations have been approved by regulatory agencies for clinical use, such as Doxil for ovarian and breast cancer and AmBisome for fungal infections [10]. Polymer-based drug delivery systems offer several advantages, including their biocompatibility, biodegradability, and ease of functionalization. Polymers can be synthesized in different forms, such as micelles, dendrimers, and NPs, and can be functionalized with specific ligands to target specific cells or tissues. The use of polymers in drug delivery has been shown to enhance drug solubility, stability, and bioavailability. For example, polymeric nanoparticles have been used to deliver anticancer drugs, such as paclitaxel, and have proved to be more efficacious than traditional chemotherapy [11]. Nanoparticles are submicron-sized particles made from different materials, such as metals, polymers, and lipids. Nanoparticles can also be functionalized with ligands targeting specific cells or tissues and can be used to encapsulate drugs to improve their solubility and stability. The advantages of using NPs in drug delivery are an improved drug bioavailability, a reduced toxicity, and the capability of crossing biological barriers, such as the blood–brain barrier. Several NP-based drug delivery systems have been approved for clinical use, such as Abraxane for breast cancer and Onpattro for hereditary transthyretin-mediated amyloidosis [12].

Nanoparticle size is an important parameter for many applications of NPs, including imaging, catalysis, and development of advanced drug delivery systems, and has been a subject of research in the field of medical NP applications for many years [13]. The main areas of the use of nanoparticles are shown in Fig. 1.

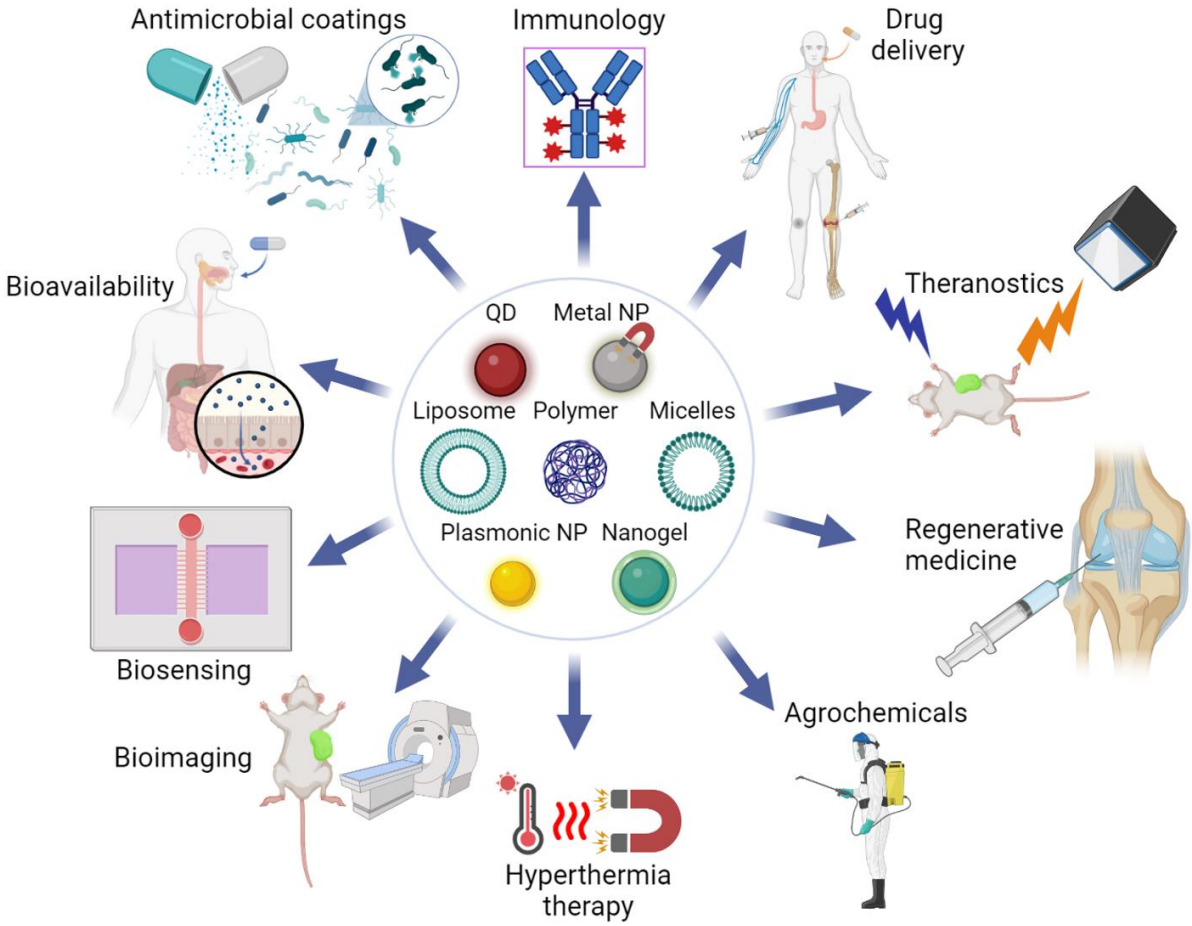


Fig. 1 Applications of nanoparticles in biomedicine sphere.

The size of NPs can affect their physical, chemical, and biological properties, which can, in turn, affect their behavior and performance in different applications. In drug delivery, e.g., the size of NPs can affect their capacities for circulating in the bloodstream, penetrating biological barriers, and interacting with target cells or tissues. Smaller NPs usually have longer circulation times, they better penetrate barriers but may also be more susceptible to clearance by the immune system. Larger NPs usually have longer circulation times, but they may be less capable of penetrating biological barriers or interact with target cells or tissues. In imaging, the size of NPs may affect their contrast properties, such as brightness and resolution [14]. Overall, understanding the size-dependent properties of NPs, ζ-potential, polydispersity, and concentrations is crucial for their effective use in various applications and can help in designing more efficient and effective NP-based systems.

The DLS method employs the interaction of monochromatic coherent radiation with light-scattering particles in the solution studied. Analysis of scattered radiation spectra in the DLS method is based on the Rayleigh scattering theory, Fraunhofer theory and the Mie theory. In the general case, the interaction of the light with a particle in the solution may lead to diffraction, refraction, reflection, and absorption. If the characteristic particle size is larger than the incident light wavelength, the diffraction process described by the Fraunhofer theory is predominant, and if the characteristic particle size is smaller than the wavelength of the scattered light, elastic light scattering without wavelength change occurs, which is described by the Rayleigh scattering theory [15]. Radiation scattered by particles whose size is comparable to the wavelength is detected at large angles (more than 90°) and is described in terms of the Mie theory. The DLS technique is implemented in various devices differing in optical configuration, signal modulation and analysis, detection system, and sensor geometry. The differences in design do not so much affect the calculated data or intensities of the measured signal, but rather determine the differences in operating concentration ranges, sensitivity of devices to certain sizes of objects, achievable resolutions of size distributions, and methods of data processing and signal analysis, which directly affects the measurement error and the results of measurements.

This review considers examples of using the DLS method in recent studies of biopolymers, NPs, and microparticles of various types, as well as interactions between them, to establish the relationships between the detected parameters and the properties of the objects studied. The concluding section of the review provides details on the application areas of the DLS method, its advantages and inherent limitations, and comparison with other optical methods of biomolecule analysis.

## 2 Theoretical Basis of the Dynamic Light Scattering Method

The DLS method is based on analysis of changes in incident radiation parameters, including the frequency and intensity, as well as the directional diagram, which changes or fluctuates when light passes through a layer of Brownian particles [16]. In this case, interference of individual scattering waves (signals) may lead to signal fluctuations on the radiation detector. The principle of DLS method is schematically shown in Fig. 2.

In the standard implementation of the DLS method, the sample or system studied is laser-irradiated, and the scattered light is detected at a certain scattering angle θ.

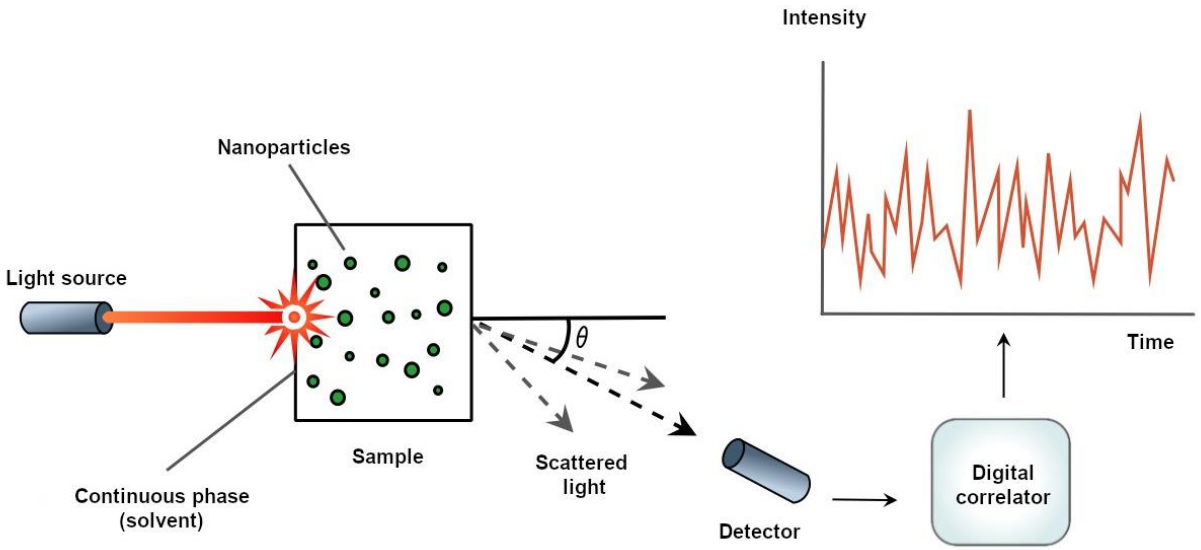


Fig. 2 The principle of the dynamic light scattering method. Light scattered by nanoparticles irradiated by a laser is measured with a high time resolution at a certain angle θ; the scattering signal fluctuation reflects the dynamics of microstructural processes, such as the Brownian motion of the particles.

The scattered radiation is either directly received by the detector or is superimposed or "mixed" with the reference signal reflected from the sample surface with an unshifted frequency. The power of the resultant signal is proportional to the product of the intensities of the scattered and reference signals. This makes it possible to detect low-power scattered radiation, which is important in studying nanometer-sized particles. The measured size of particles should not depend on the concentration of the sample. The use of backscatter detection allows a wider range of concentrations to be measured accurately compared with the standard operating procedures with the detection angle $\theta = 90°$ [17]. According to the first approximation of the classical theory of radiation, a pair of interacting molecules or NPs can be considered as a time-varying dipole that emits electromagnetic radiation. As such, the NP behaves like a secondary light source and scatters light. This scattered light is fully polarized at 90° to the incident beam, and its intensity ( $I_0$ ) is proportional to the diameter ($d$) of the analyte ($I_0 \propto d^6$) and its polarizability [18]. The polarization of light scattered from particles with various shapes was described by Damaschke et al. [19]. Thus, the DLS method requires the use of colloidal suspensions with low concentrations to avoid the effects of secondary scattering and destructive interference.

Typical dynamic light scattering instruments use a detection angle of 90°, which may be not sensitive enough to measure small particles or molecules even with the use of a high-powered laser at a small wavelength. Backscatter detection is an optical configuration that can measure samples with smaller sizes and lower concentrations. At $\theta = 173°$, the scattering volume detected at the detector is about eight times greater than in the case of the traditional 90° optics [20]. This leads to an eightfold increase in the detected count rate, which is directly related to the instrument sensitivity to small particles at lower concentrations. Depending on the experiment, the angle $\theta$ can vary and reach, e.g., 175° [21]. The use of fiber optics in combination with this optical setup ensures that the signal-to-background ratio or the intercept of the correlation function is not degraded at high detection volumes, in contrast to the traditional geometric optics ($\theta = 90°$). Maintaining the count rate while reducing the intercept of the correlation function is crucial. This optical configuration provides the exceptional sensitivity necessary for measuring the size of NPs and molecules at low concentrations.

Regardless of the version of the DLS method, the general principle is that the analysis of the detected signals takes into account their fluctuations, whose duration is determined by the Brownian motion of particles and lies in the range from nano- to milliseconds. Analysis of the DLS signals assumes that the scattered light is coherent, but the classical DLS setup cannot distinguish between coherent and incoherent signals, which are mainly caused by multiple scattering. This calls for alternative analytical methods, e.g., cross-correlation techniques [22].

In this review, we consider the main uses of the classical DLS method in various fields. The use of the dynamic light backscattering method and new DLS approaches have been described by Malm et al. [23] and Hou et al. [24].

In addition, the laser self-mixing interferometry (SMI) and laser feedback interferometry (LFI) methods [25, 26] should be mentioned. The interferometric technique enables a laser to act as both a source and a detector. The operating principle of the laser techniques is the interference of light waves that are emitted and then reflected back to the laser cavity by an external target. The resulting frequency shift, which is proportional to the displacement of the target, is detected as a phase shift in the laser output signal. This signal can be used to determine the position, velocity, and acceleration of the target [27].

There are also various speckle-based methods. This is a class of optical methods that use the speckle structure formed by coherent light scattered by a rough or dynamic surface to extract information about the object or system under study. One of the most commonly used speckle-based techniques is speckle pattern correlation, which measures the displacement of speckle patterns obtained upon two separate measurements of the same object or system [28]. However, this class of optical research methods requires the development of time-consuming algorithms for data analysis [29]. All these methods have been used in various biomedical applications, including measuring the thickness and mechanical properties of biological tissues and detecting blood flow in blood vessels. Although some optical techniques share similarities with the DLS method, we do not discuss them in detail here, because they are not commonly used for characterizing microparticles, NPs, or polymers.

## *2.1 Light Absorption and Scattering by an Arbitrary Particle*

All media except for vacuum can be considered, in a sense, heterogeneous. Even the media that are regarded homogeneous, such as pure gases, contain some local inhomogeneities – these are atoms and molecules. Consequently, all media will scatter light due to these local inhomogeneities. When an electromagnetic wave passes a system, each particle in the system is affected not only by the incident wave, but also by the sum of secondary fields generated by all other molecules in the medium. Under nonideal conditions, the average number of molecules in a given area of the system at any moment of time differs from that at the preceding moment. Precisely these density fluctuations lead to scattering in dense media. There are also concentration fluctuations, which also lead to scattering. If molecules have an irregular (nonspherical) shape, then orientation fluctuations occur. With clusters of particles, the situation is more complicated, because each particle is excited by an external field and resultant field scattered by all the other particles. In this case, the field scattered by the particle directly depends on the field in which it

is placed. When dealing with a cluster of charged NPs, we should bear in mind that this group of particles may display specific optical properties, which may drastically differ from the optical properties of NPs measured in a classical colloidal solution. For example, a spiral arrangement of gold NPs (GNPs) results in circular dichroism [30]. Interacting metal NPs exposed to an external electromagnetic wave exhibit a greater amplification of the electric field compared to isolated metal NPs, as well as a shift of the resonance peak and a change in scattering direction with changing distance between the particles [30].

When a particle is irradiated by a light beam with given characteristics (wavelength, incident angle, and temporal and spatial coherences), the amount of scattered light and its angular distribution, as well as the amount of absorbed radiation, directly depend on the particle shape, size, and composition. Light scattered by a single particle or a set of particles with the same shape, composition, size, and orientation is completely polarized. In this case, the intensity of scattered light is maximal if the wavelength of incident radiation is of the same order as the size of the examined object. If the inhomogeneities are small-sized compared to the wavelength of light, the intensity of the scattered light is proportional to the fourth power of the frequency or inversely proportional to the fourth power of the wavelength [31]. This relationship is called Rayleigh's law:

$$I \sim \omega^4 \sim \frac{1}{\lambda^4}, \tag{1}$$

$$I = I_0 \frac{9\pi^2 \varepsilon_0^2 N \tilde{V}^2}{2\lambda^4 L^2} \left(\frac{\varepsilon - \varepsilon_0}{\varepsilon + \varepsilon_0}\right)^2 (1 + \cos^2\theta), \tag{2}$$

where $I$ and $I_0$ are the intensities of the scattered and incident radiations, $N$ is the number of particles in the light-scattering volume, $\tilde{V}$ is the particle volume, $\varepsilon$ is the dielectric constant of the particles, $\varepsilon_0$ is the dielectric constant of the medium where the particles are suspended, $\theta$ is the scattering angle, $L$ is the distance between the scattering volume and the observation point, and $\lambda$ is the wavelength of nonpolarized incident light.

Thus, Rayleigh scattering is coherent scattering of light which does not change the incident wavelength on particles or inhomogeneities. This type of scattering is termed elastic scattering. The vibrational electric field of incident light induces an oscillatory dipole moment in the particle, which subsequently emits light in the characteristic zone described by the dipole radiation pattern. For example, in the case of a spherically symmetric particle and linearly polarized light, the induced dipole moment is parallel to the direction of incident light polarization and is proportional to the polarizability of the particle.

## *2.2 Light Absorption and Scattering by a Spherical Particle*

The Mie scattering theory is a complete solution of Maxwell's equations for scattering of electromagnetic waves on spherical particles and predicts the intensity of scattering induced by all particles in the measurement range [32]. It can be used to analyze the characteristic intensity distributions for small particles (in this case particle size is comparable with wavelength of the scattered light), which, in contrast to those predicted by the Fraunhofer theory, are not limited to scattering angles smaller than 90° (forward direction) but can be also calculated for scattering angles larger than 90° (backward direction). For calculating the particle size on the basis of the intensity distribution determined in this way, the Mie theory, in contrast to the Fraunhofer theory, requires that the refractive index and the absorption coefficient of the material studied be known. It is worth clarifying that for particles (with size $a$) that are significantly greater than the wavelength ($\lambda$) of the scattered light ($a \gg \lambda$), and with refractive indices that are substantially different from the unity, the scattering light can be accurately describe by Fraunhofer diffraction theory [33]. This theory valid for particles of size greater than several μm when analyzed with visible light [34]. When not all the optical properties of the nanoparticles are known, Fraunhofer is used since it is an approximation to the Mie theory. However, in the case of small or transparent particles, the use of the Fraunhofer approximation leads to an error in the size measurement [35].

The cross section of electromagnetic wave scattering on a particle depends on the ratio between the particle size and the incident wavelength, as well as the change in the light wavelength upon interacting with the particle material [36]. Rayleigh scattering is a special case of Mie scattering when the particle is much smaller than the wavelength. In this case, the external electromagnetic wave polarizes the particle, exciting an oscillating dipole moment in it. The dipole moment, whose oscillation is synchronous with the frequency of the external wave, re-emits light with a radiation pattern characteristic of the dipole moment. The Mie theory and Mie coefficients are described in more detail in Ref. [37]. As an electromagnetic wave effect is an external perturbation, we can use physical formalism to analyze the forces and moments acting on the object. If the size of this object is between the Rayleigh and geometric optics limits, its original form considers the scattering of a plane wave by a spherical particle and generalization of the Lorentz–Mie scattering is required. Whereas the Mie theory is more suitable for analyzing charged NPs in a solution [38], the generalized Lorentz–Mie theory describes the scattering of arbitrary fields [39] and makes it possible to find exact solutions for the scattering of plane waves by individual dielectric spheres in arbitrary frequency modes [40]. The differences between Rayleigh scattering and Mie scattering are shown in Table 1 and Fig. 3.

Table 1 Differences between Rayleigh scattering and Mie scattering.

| Rayleigh scattering | Mie scattering |
|---|---|
| Fluctuation of the concentration may affect the refractive index. | The suspension is strongly diluted, and light can be considered to be scattered by a single particle and detected before it has interacted with other particles. |
| The scattering strongly depends on the incident wavelength. | The scattering weakly depends on the incident wavelength. |
| The particle size ($a$) is smaller than the incident wavelength [41]: $a \le \frac{\lambda}{10}$ The scattered light carries the same energy (elastic scattering) as the incident light and is independent on the angle. | The particle size ($a$) is about the same as, or larger than, the incident wavelength [41]: $a > \frac{\lambda}{10}$ Rayleigh scattering is replaced by the anisotropic Mie scattering, with the scattered light energy unequal to the incident light energy (inelastic scattering) and depending on the angle; i.e., the scattered light is more intense along the direction of the incident light. |

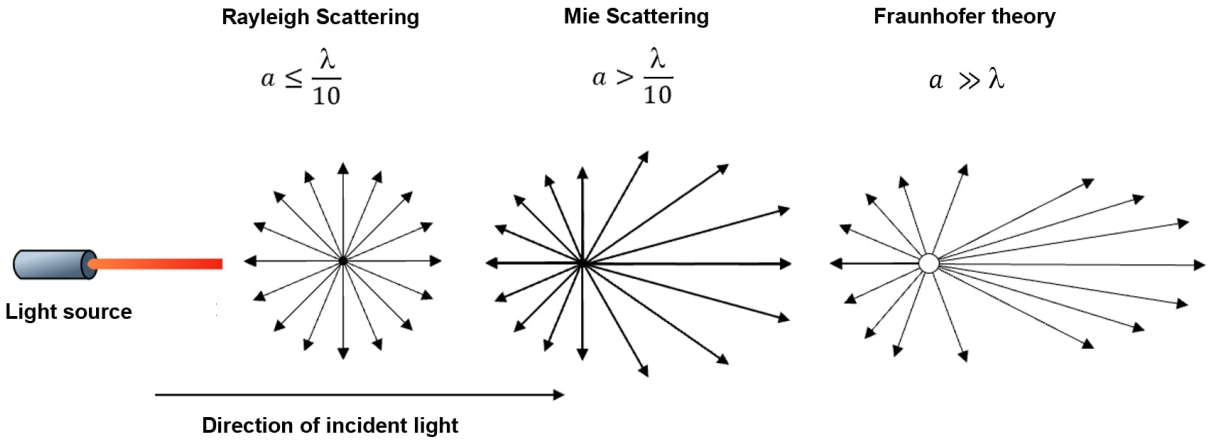


Fig. 3 Differences between Rayleigh scattering and Mie scattering; $a$ is the characteristic size of the particles studied.

According to Yue et al. [42], disperse NPs scatter incident light proportionally to the sixth power of their radius ($I \propto d^6$). In this case, the intensity distribution has the form:

$$I = I_0 \frac{1+\cos^2\theta}{2R^2}\left(\frac{2\pi}{\lambda}\right)^4\left(\frac{n^2-1}{n^2+2}\right)^2\left(\frac{d}{2}\right)^6, \quad (3)$$

where $I$ and $I_0$ are the intensities of the scattered and incident radiations, $R$ is the distance between the scattering volume and the observation point, θ is the scattering angle, λ is the wavelength of nonpolarized incident light, $d$ is the particle diameter, and $n$ is the absolute refractive index of the medium.

## 2.3 Brownian Motion

The behavior of colloidal particles is described by the kinetic molecular theory, which assumes that spherical particles diffuse in a liquid phase consisting of molecules small enough for this phase to be considered as a continuous medium. Then, Brownian motion of particles results in self-diffusion of molecules in the liquid medium, whose coefficient is estimated using the Stokes–Einstein equation [43]:

$$D_p = \frac{k_B T}{3\pi\eta r_{h,t}}, \quad (4)$$

where $D_p$ is the diffusion coefficient of the particles, η is the dynamic viscosity of the liquid, $r_{h,t}$ is the hydrodynamic radius (HR) of translationally moving particles, $T$ is the temperature of the colloidal solution, and $k_B$ is Boltzmann's constant.

The HR (Stokes radius) is the size of an object that is calculated from its diffusion coefficient in a liquid, on the assumption of its spherical shape. For spherical particles, such as components of sols and latexes, the real size is almost the same as the HR. For nonspherical particles, such as ellipsoids, cubes, rods, or particles with through holes, the HR is a conditional or effective parameter.

Brownian motion is a continuous chaotic motion of particles of the dispersed phase caused by hits from the molecules of the solvent (dispersion medium), which are in the state of intense thermal motion. The particles of the dispersed system, repeatedly hit by fluid molecules from different sides, can translationally move in different

directions. The Einstein–Smoluchowski equation shows [44] that the mean squared displacement of a particle in the case of one-dimensional Brownian motion during the time ($t$) is equal to following:

$$\overline{\Delta x^2} = 2D_p t, \tag{5}$$

where $D_p$ is defined by Eq. (4).

The chaotic Brownian motion of dispersed particles leads to microscopic fluctuations of the particle concentration in local points of space and the corresponding local inhomogeneities of the refractive index of the medium. When a laser beam passes through the medium with local inhomogeneities, part of the light will be scattered on these inhomogeneities. The fluctuations of the intensity of scattered light will correspond to the fluctuations of the local concentration of dispersed particles. Information about the diffusion coefficient of particles is contained in the time-dependent correlation function of the intensity fluctuations detected by the detector, and it depends on the fluctuations of the particle coordinate in the solution (see Fig. 4).

Frequency analysis or correlation spectroscopy can be used for qualitative and quantitative estimation of scattering signal fluctuations. Frequency analysis decomposes the signal into its frequency components to obtain the frequency distribution or the spectrum of the power $P(\omega)$ [45]:

$$P(\omega) = \lim_{T\to\infty} \frac{2}{T} \left\langle \left| \int_0^{\frac{T}{2}} I_{det}(t) \cdot e^{-i\omega t}\, dt \right|^2 \right\rangle, \tag{6}$$

$$P(\omega) = \int_0^{\infty} \langle I_{det}(t) \cdot I_{det}(t + \tau) \rangle e^{i\omega t}\, dt,$$

where $I_{det}(t)$ is the detected light intensity, $\tau$ is the delay time between two scattering signals, $\omega$ is the carrying frequency, and $i$ is the imaginary unit.

By definition, the time autocorrelation function has the following form [46]:

$$g_2(q,\tau) = \frac{\langle I_{det}(t) \cdot I_{det}(t+\tau) \rangle}{\langle I_{det}(t) \rangle^2}. \tag{7}$$

The autocorrelation function $g_2(q,\tau)$ in Eq. (7) quantitatively defines the time-averaged correlation between two scattering signals measured at the time delay $\tau$.

In a system of monodisperse particles with single scattering where Brownian motion occurs, the corresponding correlation function is represented as a sum of a constant and a damped exponential, e.g.,

$$g_2(q,\tau) = A + B \exp\left(-C \cdot D_p q^2 \tau\right), \tag{8}$$

where $q$ is the scattering amplitude; $\tau$ is the time interval between measurements; and $A$, $B$, and $C$ are constants.

On the other hand, the first-order correlation function of the electric field is exponentially damped in the case of Brownian motion of monodisperse particles:

$$g_1(q,\tau) = \exp(-\Gamma \cdot \tau). \tag{9}$$

For polydisperse particles, the equation takes the following form:

$$g_1(q,\tau) = \int_0^{\infty} \exp(-\Gamma \cdot \tau) dQ_{int}(\Gamma), \tag{10}$$

where $\Gamma$ is the time coefficient of the decrease in particle size in the medium and $dQ_{int}(\Gamma) = A_i = const$ is the weight coefficient defining the relative contribution to the scattering intensity.

$$\Gamma = q^2 D_p. \tag{11}$$

The Euclidean norm of the scattering vector $\vec{q}$ [47] is

$$q = \|\vec{q}\| = \frac{4\pi n}{\lambda_0} sin\left(\frac{\theta}{2}\right), \tag{12}$$

where $n$ is the refractive index of the disperse medium, $\lambda_0$ is the wavelength of incident light (a laser beam) in vacuum, and $\theta$ is the scattering angle.

Eq. (10) can be rewritten in the form:

$$g_1(q,\tau) = \int_0^{\infty} A(\Gamma) \cdot \exp(-\Gamma \cdot \tau) d\Gamma, \tag{13}$$

where $A(\Gamma) \cdot d\Gamma$ is the proportion of the correlation function damped with time of inverse relaxation between $\Gamma$ and $\Gamma + d\Gamma$.

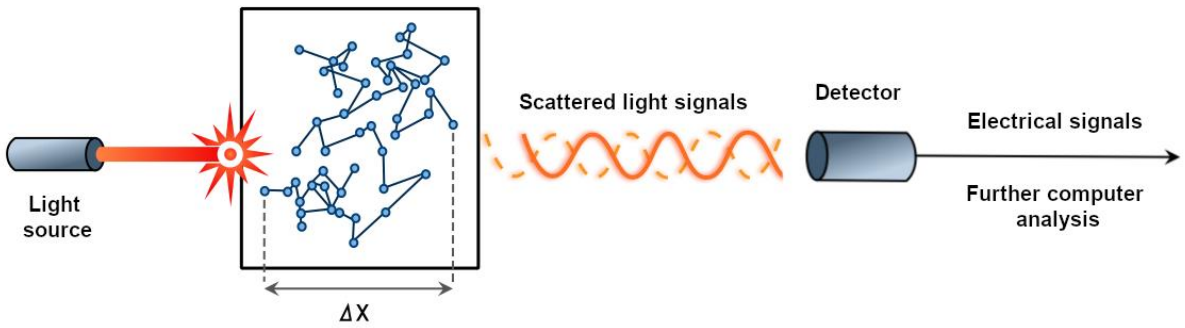


Fig. 4 Fluctuation of the particle position in a colloidal solution.

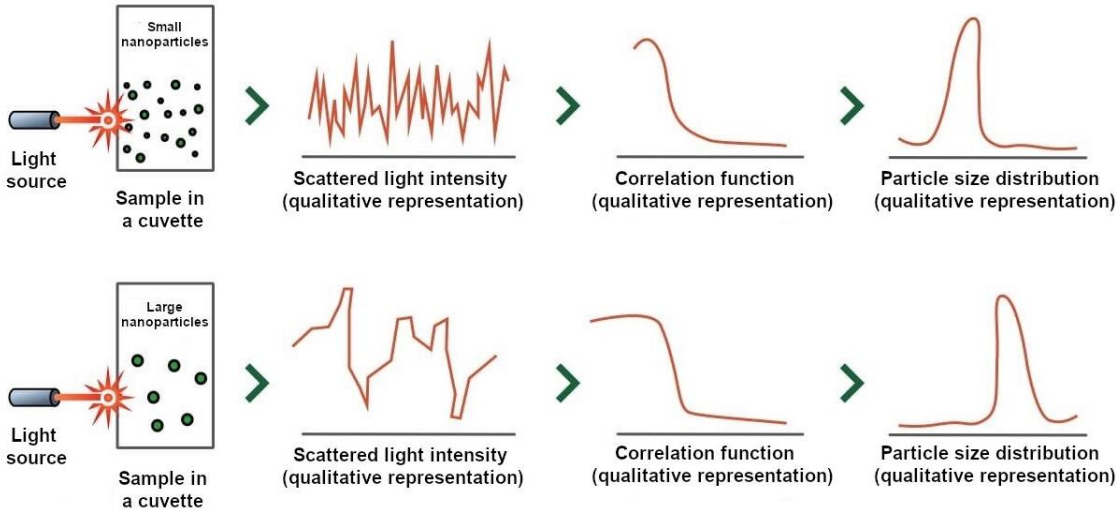


Fig. 5 The qualitative presentation of the data obtained using dynamic light scattering.

The coefficients at the exponent depend on the contribution to the total intensity of the scattered light and the intensity of the light scattered on particles of the same size. To determine the correlation times from the experimental correlation function, we need to select a set of times and coefficients in Eq. (13) so that the difference between the calculated and experimental functions tend to the minimal value. It should be noted that Eq. (13) in its general form belongs to the class of integral equations and, in our case, represents the Fredholm integral equation of the first kind. Its solution belongs to the class of incorrectly set problems [48]. This means that, if the function $g_1(q,\tau)$ is defined with a small error, the solution may differ from the true one and may not be the only one. Within the experimental error, there will be an infinite number of different solutions that fit the experimental data well. The more accurate the experimental data, the fewer solutions will fit these data. Thus, knowing the form of the correlation function, one can obtain the particle size distribution by using a software (mathematical algorithm) [49]. Fig. 5 shows the qualitative presentation of the results obtained by the DLS method.

There are also NPs whose motion does not obey the Stokes–Einstein relation. The DLS estimation of the particle size distribution assumes that the scattered light fluctuates only because the particles are continuously displaced due to Brownian motion. When DLS is used to quantify the properties of individual particles, the sample should be diluted as much as possible to exclude any influence of the particle concentration, otherwise the estimates may considerably deviate from the actual values, and the measurement error will be high.

Several factors that determine the difference between the real and the ideal experimental situations are: (i) multiple scattering within the sample; (ii) nonrandom spatial distribution of particles; (iii) viscous interaction between neighboring particles; (iv) signal fluctuation that reflects not only the Brownian motion of individual particles, but also stochastic variation of the local concentration of particles; (v) signal fluctuation determined by Brownian displacement on short- and long-time scales; (vi) possible coagulation of particles.

The results of the analysis also depend on the properties of the particles (size, shape, and optical properties) and the medium (phase boundary properties), as well as the parameters of the measuring instruments (wavelength and scattering angle). However, in the case of nonspherical particles, one more factor, Brownian rotation of the particles, inevitably contributes to the signal fluctuation. The rotation affects the spatial orientation of the particles and, hence, the scattering of light in a given direction.

It should also be borne in mind that the characteristics of the Brownian motion of particles can be influenced by surfactants. These are substances that are positively adsorbed at the phase boundary, forming an adsorption layer with an increased concentration. A surfactant may significantly affect the diffusion coefficient, which additionally alters the Stokes–Einstein relation, so that the relation does not hold for this type of systems. This effect has been observed experimentally, e.g., in a reverse micellar system containing 15 wt.% of polydisperse hexaethylene glycol monodecyl ether ( $C_{10}E_6$ ) in cyclohexane [50]. As a result, the correction coefficients for the viscosity and self-diffusion of particles were determined to fit the experimental data to the Stokes–Einstein relation.

In the general case, the estimated hydrodynamic diameter of nonspherical particles is correlated with the scattering angle [49]. Hence, the systemic dependence of the measured size distribution on the scattering angle suggests a nonspherical shape. Note that the effects of nonspherical shape remain hidden for DLS devices with only one scattering angle.

Characterizing the motion of particles in a medium is generally a difficult task, and it is further complicated by characteristic hydrodynamic interactions (HIs) mediated by the solvent and suspended particles. Therefore, HIs affect the dynamics of the spheres and considerably

complicate the calculations. HIs are usually long-range, non-pairwise-additive forces occurring at high particle concentrations [51].

Short-term diffusion is defined as diffusion of colloidal particles investigated over a time interval $t$ satisfying the following two inequalities [52]:

$$\tau_H \sim \tau_I \ll t \ll \tau_D, \quad (14)$$

where $\tau_H$ is the hydrodynamic time scale that quantitatively defines the interval in which shear waves of the solvent cross the characteristic distances between (larger) colloidal particles, $\tau_I$ is the time of impulse relaxation, and $\tau_D$ is the time interval of diffusion interaction described in terms of the Stokes–Einstein free translational diffusion coefficient.

Inequalities (14) define the short-term colloidal mode, which takes into account the times of impulse relaxation and diffusion interaction of the particles. At time moments $t \gg \tau_I$, many random collisions of the colloidal particle with solvent molecules occur, the particle motion is diffusive, and inertia does not play any role. During the time $t \gtrsim \tau_D$, diffusion considerably changes the spatial configuration of (smaller) particles compared to their original configuration, and, in addition to HIs, permutations of groups of neighboring particles begin to affect the dynamics of the particles in the medium. This leads to a subdiffusive particle motion at the time moment $t \gtrsim \tau_D$ preceding the finite diffusive long-term mode $t \gg \tau_D$, in which the particle can occupy many independent local regions.

The function of the scattering wavenumber $q$ and the correlation time $t$ is a fundamental quantity determined in DLS experiments. It represents the normalized intermediate scattering function $f_c(q,\tau)$ [51]:

$$f_c(q,\tau) \approx \exp(-q^2 \cdot D_s(q)\tau), \quad (15)$$

where $D_s(q)$ is the short-term diffusion function proportional to the hydrodynamic function $H(q)$. The hydrodynamic function serves as a generalized short-term sedimentation coefficient and directly reflects HIs. In the case of infinite dilution or (hypothetical) absence of particles, the function $H(q)$ is identically equal to unity [51].

Attempts at computer model of the process described above have been made [51, 52]. In general, the dynamic scattering functions obtained in Stokes dynamics simulations [53] agree well with the results of DLS for a range of concentrations of charged spherical silicon NPs in a mixture of organic solvents within certain experimental time range and wavenumber range. There are many approaches to determining the characteristic particle size, in particular, estimations based on the diffusion coefficient calculated from data on polydisperse samples. Most of these approaches rely on a known analytical distribution and adjust the variables so as to obtain the best fit to the experimental data. The main problem of these methods is the a priori assumption on a given form of distribution, which often leads to ambiguous results.

## *2.4 Variants of the Dynamic Light Scattering Method*

The DLS method has some interesting variants. One of them is the multipolarization dynamic light scattering (MPDLS) method, which is based on two similar methods, multi-angle dynamic light scattering (MADLS) and depolarized dynamic light scattering (DDLS), but is essentially a new method combining the advantages of the other two. The MADLS analysis integrates information on the scattering angle from the Mie theory and analysis of the particle size distribution based on DLS measurements. Lower noise and, hence, a lesser smoothing provide a more reliable and accurate representation of the particle size distribution and better characterization of the individual components of a multicomponent sample. The MADLS method provides additional information about the sample by combining DLS measurements made from different angles. An example of comparison of the DLS and MADLS data is presented in Ref. [54]. The DDLS method provides, in addition to data on radius distributions, information on the shape of the particles. The DDLS analysis is widely used for calibrating nonspherical NPs, such as nanorods, nanowires, and nanotubes. Detailed theoretical basis of this method has been presented by Geers et al. [55]. The depolarized component of the light-scattering signal makes it possible to estimate both translational and rotational diffusions of nonspherical NPs. As a result, the DDLS method determines not only the HR of the equivalent sphere, but also the actual length and diameter of diffusing NPs [56]. By considering the Brownian motion of NPs in terms of translational and rotational diffusions, the particle sizes can be determined from the rates of damping of the scattered-light fluctuations. The damping rates are determined for light scattered with two different polarizations, one of which (co-polarization) coincides with the polarization of the excitation light and is termed the VV component (vertically polarized waves transmitted and received) and the other (cross-polarization) is perpendicular to it and is termed the VH component (horizontally polarized waves transmitted and only vertically polarized waves received) (see Fig. 6). The depolarized component, e.g., the horizontally polarized one in the case of vertically polarized incident light, results from multiple DLS and is usually weak. It disappears in the case of spherical particles in dilute suspensions. Thus, the MPDLS method differentiates between the translational Brownian motion of particles from the Brownian rotation and provides the shape parameters of the particles in addition to their sizes [49].

Diffusing wave spectroscopy (DWS) is also based on DLS. The concept behind this method is that the motion of scattering particles influences the coherence of the light scattered by them.

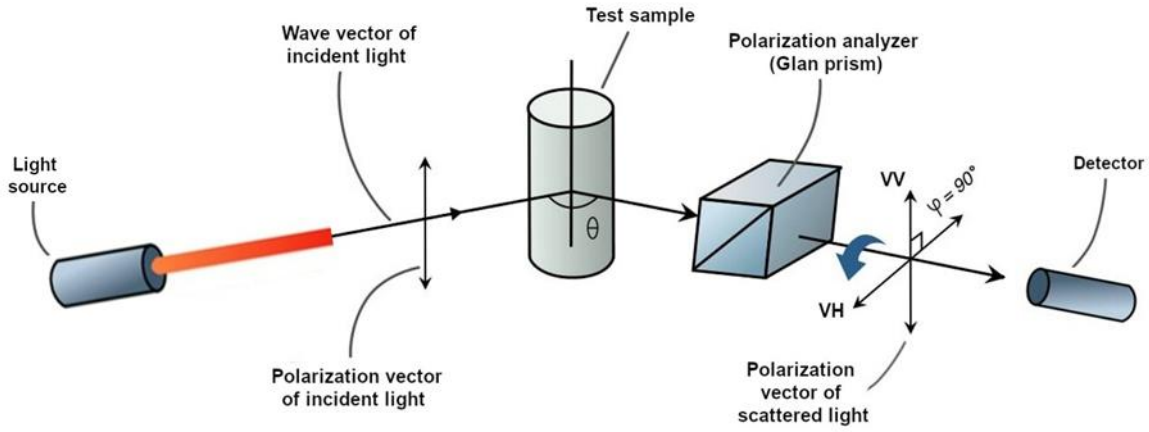


Fig. 6 A method of depolarized dynamic light scattering measurement scheme.

By analyzing the temporal fluctuations of scattered light, the diffusion properties of the particles can be determined. In contrast to the DLS method, which measures the intensity fluctuations of scattered light, the DWS method measures the temporal fluctuations of the speckle pattern of the scattered light, which ensures more robust measurements. One of the primary applications of DWS in biomedicine is the measurement of the size and shape of NPs and molecules [57].

## 3 Specifics of the Dynamic Light Scattering Analysis of Nanoparticles and Polymers

This section describes examples of the use of DLS in biochemistry, with the focus on important specifics of studying samples of different types and some guidelines to these studies.

### *3.1 Measurement of Nanoparticle and Polymer Sizes*

DLS size measurements are based on measuring the time parameters of light fluctuations on the detector caused by random diffusion or motion of suspended particles in a small "scattering volume". The scattering volume is defined as the volume inside the sample illuminated by the laser beam from which the light scattered by particles directly goes to the detector. Small particles diffuse rapidly, leading to rapid fluctuations of intensity at the detector; large particles diffuse more slowly, causing longer fluctuations of scattered light at the detector.

The size of NPs is known to affect their distribution, sites of accumulation, and routes of elimination from the body, as well as their possible toxic effect [58]. At the same time, NPs are increasingly used in cosmetic products as sunscreens, which requires a low-cost method of controlling the size of NPs in creams. De la Calle et al. [59] have compared different analytical methods used for determining the size of NPs in cosmetic products. The DLS method quickly determined the HR of NPs and their size distribution, but the size was overestimated because of the solvation layer on the NP surface and the high viscosity of the samples. It was found that the discrepancy between the experimental data and real NP sizes in analysis of fat samples could be reduced by treating the suspensions with 0.1% sodium dodecyl sulfate or precipitating the NPs with hexane, with subsequent removal of the hexane solution and dissolution of the precipitate in distilled water. The DLS method is readily applicable to analyzing the size of dispersed liposomes and micelles intended for drug delivery. Chan et al. [60] have developed a protocol for analyzing nanoemulsions of oil in water by the DLS method, thus having shown that the DLS method is suitable for studying objects other than solid particles.

One example of an application of DLS is the study of colloidal stability of charged NPs in the presence of oppositely charged surfactants, such as cetyltrimethylammonium bromide and dodecyltrimethylammonium chloride. In this case, the DLS method can be used to determine not only the colloidal stability, but also the charge of NPs, and, hence, to infer the structure of NPs coated with charged surfactant ligands [61]. Now that a growing number of various biological imaging studies use NPs as contrast agents [62], it is important to explore the interaction of NPs with proteins. Moerz et al. [63] studied how GNPs with a citrate-functionalized surface formed stable hybrid clusters with hemoglobin. In that study, DLS analysis was used to estimate the sizes of not only GNPs, but also the hemoglobin–GNP clusters. Note that the use of DLS analysis allowed the researchers to determine minimal concentrations of clusters formed upon adding as little as 0.1 mg/L of hemoglobin, which indicates a high sensitivity of the method.

The DLS method is widely used to determine the hydrodynamic sizes of NPs of different compositions and with different surface ligands (Table 2). In addition, DLS analysis is suitable for studying changes in the size and morphology of GNPs exposed to strong laser radiation.

These studies are especially important because there are examples of using NPs for hyperthermal destruction of tumors [69], and it is essential to control the possible size of the NPs after their heating with laser irradiation.

Table 2 Hydrodynamic diameters of different nanoparticles determined by the dynamic light scattering method.

| Nanoparticle type | Surface ligand | Hydrodynamic diameter, nm | Ref. |
|---|---|---|---|
| $Fe_3O_4$ | Poly(sodium(4)-styrenesulfonate) | ~200 | [64] |
| | Poly(diallyldimethylammonium chloride) | 107.4 ± 53.7 | [65] |
| | Mercaptosuccinic acid | 78.48 ± 0.91 | [66] |
| $\varepsilon - Fe_2O_3$ | Poly(4-vinylpyridine)-block-poly(methoxypolyethylenglycolacrylate-co-Rhodamine polyethylenglycolmethacrylate-co-carboxylic polyethylenglycolmethacrylate) | without coating, 18 after coating, 27 | [67] |
| $\gamma - Fe_2O_3$ | | without coating, 29 after coating, 36 | |
| Au@citrate | - | 58 ± 6 | [68] |
| Au@ pMEO$_2$MA-G1 | 2-(2-Methoxyethoxy)ethyl methacrylate | 102 | |
| Au@ pMEO$_2$MA-G2 | | 177 | |
| Au@pNIPAM-G4 | N-Isopropylacrylamide | 141 | |
| Au@pNIPAM-G5 | | 197 | |
| Au@pMMA-G6 | Methyl methacrylate | 225 | |
| Au@pMMA-G7 | | 216 | |
| Au@pSt-G9 | Styrene | 102 | |
| Au@pSt-G10 | | 151 | |
| Au@pSt-G11 | | 198 | |

pMEO2MA-(G1–G11) are samples differing in the molar fraction of sodium dodecyl sulfate used during sample formation and in the molar ratio of solvents (water and ethanol).

Table 3 Effect of the solvent on the detected $TiO_2$ nanoparticle size [73].

| Organic solvent | Nanoparticle size, nm |
|---|---|
| Acetone | 642 |
| Butanol | 668 |
| Methanol | 626 |
| Isopropanol | 774 |
| Ethylene glycol | 550 |

Cavicchi et al. [70] used the DLS, DDLS, and transmission electron microscopy (TEM) analyses to determine changes in the average size and size distribution of GNPs under laser irradiation and demonstrated a high sensitivity of DLS-based techniques and good correlation of their results with TEM data for diluted solutions of 10- to 100-nm NPs. It is also worth noting that researchers who design the experiment and select its parameters should be experienced in this field, because a minor change in the experimental parameters can significantly affect the reliability of the results. For example, Zheng et al. [71] studied the effects of GNP concentration, laser radiation power, and the multiple scattering phenomenon on the estimated HR of GNPs coated with citrate ligands with a nominal size of 100 nm. Their study has shown that the estimated HRs of GNPs strongly depend on the concentration and on the power of the incident laser radiation. The intensity of scattered light is proportional to the sixth power of the NP diameter, and the extremely intense light scattered on 80-nm or larger GNPs causes a substantial multiple scattering effect in conventional DLS instruments. This effect leads to considerable errors in the detected HR in the case of routine data analysis not taking into account the multiple scattering. Other examples of experiments with gold, silver, and alloyed gold–silver NPs in aqueous media are compiled elsewhere [72].

Zhang et al. [73] studied the effect of the medium on the measurement of NP sizes by the DLS method. As an example, the sizes of $TiO_2$ NPs, originally in the powder form, were determined in different solvents (Table 3).

The above examples show the importance of selecting the experimental parameters in DLS studies and demonstrate the effects of the laser flux density and medium composition on the estimated NP size. The composition of the NPs may also influence the size estimates. For example, a strong surface plasmon resonance (SPR) on GNPs significantly increases the intensity of scattered light compared to particles of the same size and shape made from materials that do not display SPR. This is of particular importance given the widespread use of the SPR effect in the imaging of malignant neoplasms, in theranostics, and in bioimaging [74]. Lehmann et al. [75] used DLS to measure the photoinduced size changes of hybrid particles, GNPs coated with a thermosensitive polymer. They used the setup for the MADLS analysis where the particle size was determined by irradiation with a helium–neon laser (633 nm), and an additional sapphire laser (532 nm) was used to irradiate GNPs in the SPR wavelength range. The use of MADLS made it possible to obtain absolute values of the HRs of bare GNPs and GNPs coated with thermosensitive polymer and to correct the data by excluding the light scattered by the GNPs. In contrast, in a single-angle DLS experiment, the light scattered by the GNPs would dominate the signal, especially at large angles, and only relative HR values would be available. This example shows the effect of SPR on the measurement process. A similar setup could be used for studying vesicles, microgels, and other hybrid systems, e.g., in developing drug carriers that would degrade in response to irradiation. Table 4 summarizes data on the sizes of different types of NPs as estimated by the DLS, TEM, and small-angle X-ray scattering (SAXS) methods.

However, it should be remembered that direct comparison of NP sizes estimated using different techniques is not entirely correct. For example, DLS measures the HR of particles that actually consist, apart from the particles per se, of the layers of ions and solutes adsorbed from the solution, depending on the measurement conditions. We will consider the comparative advantages and drawbacks of the DLS method in more detail in the conclusion to this review.

The DLS measurement of NPs size is used in many test systems. For example, Liu et al. [79] have described a test system for detecting picomolar concentrations of free prostate-specific antigen (f-PSA), a prostate cancer biomarker, that identifies immunocomplexes of GNPs, f-PSA, and gold nanorods by the DLS method. Dai et al. [80] have reported a DLS-based method for detecting specific DNA sequences. This method uses two types of GNPs about 30 nm in size conjugated with oligonucleotides complementary to the 5' and 3' ends of the detected DNA. Here, DLS is used to detect the complex formed by two GNPs with DNA. The detection sensitivity is 1 pM, which is four orders of magnitude more sensitive compared with the methods based on light absorption measurement. At the same time, in developing DLS test systems, it is necessary to take into account inherent limitations of the DLS method. Specifically, the mean HR of an NP or a globular polymer remains constant, within the margin of error, as the concentration increases to a certain threshold, but further increase in concentration leads to a considerable decrease in the mean HR. Zheng et al. [71] analyzed the effect of the concentration of GNPs coated with citrate ligands on their HR estimated by the DLS method. With increasing GNP concentration, their estimated HR decreased from the nominal size of ~100 nm at a concentration of $5.6 \times 10^8$ GNPs/ml to ~50 nm at $5.6 \times 10^9$ GNPs/ml and further to ~3 nm in the most concentrated samples. Such a high measurement error is explained by the aforementioned effect of multiple scattering in concentrated solutions.

DLS measurement of the size of fluorescent quantum dots (QDs), which are widely used as fluorescent tags for *in vivo* and *in vitro* imaging [81], also has some peculiarities. The reason is that DLS analysis often involves laser radiation with a wavelength of about 630 nm, and CdSe QDs about 15 nm in size fluoresce in this wavelength range.

Table 4 Sizes of nanoparticles of different types estimated using the dynamic light scattering, transmission electron microscopy, and small-angle X-ray scattering.

| **Nanoparticles** | | **Actual size, nm** | **Estimated size, nm** | | | **Ref.** |
|---|---|---|---|---|---|---|
| Type | Sample | | DLS | SAXS | TEM | |
| Hollow $SiO_2/TiO_2$ nanoparticles | HNP25 | 25 | 28 ± 2 | 30.0 ± 0.5 | 26 ± 5 | [76] |
| | HNP50 | 50 | 57 ± 2 | 62.8 ± 0.5 | 59 ± 5 | |
| | HNP100 | 100 | 108 ± 2 | 101.4 ± 0.5 | 105 ± 5 | |
| Polystyrene nanoparticles | PS1 | – | 33.5 | 43.2 | 40.5 | [77] |
| | PS2 | – | 25.0 | 29.6 | 25.5 | |
| Gold nanoparticles | Au1 | 15 | 50.7 | - | 13.7 | [78] |
| | Au2 | 60 | 50.8 | - | 59.1 | |
| Silicon nanoparticles | Si1 | 50 | 153.7 | - | 43.8 | |
| | Si2 | 80 | 121.6 | - | 57.7 | |

This can distort the correlation function and lead to incorrect results. Therefore, the researcher has to prevent the overlap between the QD fluorescence spectrum and the laser radiation spectrum by using narrow-band optical filters or a laser with a different radiation wavelength [82]. Modlitbová et al. [83] studied the growth of the QD silicon shell as a function of time using the DLS and SEM methods. The authors observed only a minor discrepancy between the sizes of the shelled QDs estimated by the two methods at the initial stage of shell growth, but this discrepancy increased as the shell grew. Specifically, the difference between the estimates obtained by these methods was only about 8% before the start of shell growth and increased to 20% when the shell was formed. The explanation is simple: in the course of shell growth, the QD shape gradually deviated from spherical and the QD size became more variable, which led to incorrect results of the DLS measurements. It is important to correctly estimate the size of $CsPbBr_3$ semiconductor crystals with a perovskite structure. Due to their unique properties, perovskite nanocrystals are actively used in the production of solar cells, as well as scintillation detectors for biological imaging [84]. In determining their size by the DLS method, recommendations developed for quantum dots would be useful. Below, we will consider how the size of nonspherical NPs can be nevertheless determined.

### *3.1.1 Measurement of the Sizes of Nonspherical Nanoparticles*

If the particles are considered as homogeneous spheres, then all angular scattering data must satisfy the Mie theory. In all other cases, the Rayleigh–Gans approximation yields the best results, with root-mean-square radii calculated for the model selected on the basis of all previously known or assumed particle structures. For all interpretations based on the Mie theory or Rayleigh–Gans approximation [85], the particle samples should be fractionated before the measurement to ensure that the measurements are made in monodisperse samples. Nanomaterials of various shapes are widely used in biomedical research. The shape of NPs affects, e.g., their distribution in the bloodstream, circulation time in the body, and efficiency of cellular uptake, which is important when they are used for targeted drug delivery [86]. As mentioned above, the DLS method is the most suitable for measuring the sizes of NPs and microparticles (more precisely, their HRs) under the assumption that they are spherical. Therefore, the estimation of the HR of nonspherical NPs [87–90] is more difficult in both theoretical and practical terms. Two-dimensional materials have unique light-dynamic properties, a high heat conversion coefficient, and a large effective area-to-volume ratio. Therefore, they are of particular interest for various medical applications [91], including highly efficient drug loading [92]. Therefore, these materials are promising potential components of smart drug-delivery systems [93]. For example, $Y_2O_3$ NPs inhibit the growth of both Gram-positive and Gram-negative bacteria, and flake-like $Y_2O_3$ NPs exhibit anticancer activity [94]. For qualitative analysis of the shape of NPs under study, it is necessary to develop mathematical models and introduce correction factors determining the HR of NPs of different shapes [42]. Thus, when dealing with nonspherical structures, a correction factor should be taken into account. In the given example, this coefficient was so selected that the transverse size of a square-shaped NP and a circular nanoplate was 1.96 and 2.667 times the HR of their equivalent sphere [42]. With these correction factors, the DLS method can be used to accurately measure the lateral sizes of two-dimensional or nonspherical NPs. The following equation for calculating the HR of cylindrical particles is an example of the use of a correction factor:

$$R_h = \frac{3}{4}d^2\left[\begin{array}{c}\sqrt{d^2+L^2}+\frac{d^2}{L}\times \\ \times \ln\left(\frac{L}{d}-\frac{1}{d}\sqrt{d^2+L^2}\right)-L\end{array}\right]^{-1}, \quad (16)$$

where $L$ is the thickness and $d$ is the diameter of the particle.

However, complex mathematical calculations are not always necessary. For example, Lotya et al. [95] studied solutions of graphene, $MoS_2$, and $WS_2$ nanoplates with sizes ranging from 40 nm to 1 μm. They have shown that good calibration curves can be plotted with an error between the DLS (in the backscatter mode, at an angle of 173°) and TEM data of less than 40%. Thus, it sometimes suffices to plot calibration curves for NPs of different shapes and sizes in different solutions and use them to determine the size of nonspherical NPs and microparticles by the DLS method.

It should be taken into account that even small hollows and non-uniformity of shapes lead to significant divergence of DLS results from actual values. Experiments with nonspherical silver NPs with a nominal diameter of about 50 nm have shown that DLS significantly overestimates the size distribution, and primary study of unknown samples should always combine DLS with electron microscopy or a similar method [96]. Alternative methods for estimating the size of nonspherical silver NPs are summarized in Ref. [97].

Gold nanorods are a convenient biomedical material because they bind amino and thiol groups of biomolecules, thus facilitating functionalization and bioconjugation involved in the fabrication of hybrid imaging and therapeutic systems [98]. In addition, gold nanorods, due to their effective radiation absorption in the near-infrared spectral range, are ideal candidates for photothermal destruction of tumor cells [99]. The optical properties of gold nanorods and their distribution in the body depend on their size and length-to-diameter ratio, which makes the measurement of their sizes a topical task. Levin et al. [56] used the MPDLS method to determine the size of gold nanorods. Their technique was based on time-resolved measurements of the intensity of light scattered by the NPs for different angles between the directions of incident and scattered light

polarizations. Experiments with gold and iron oxide nanorods were performed. The lengths and diameters of gold nanorods estimated from diffusion coefficients using the simple Kirkwood diffusion model agreed with the TEM data. However, this was not the case for iron oxide nanorods, most likely because their shape was far from cylindrical. To determine the size of axisymmetric nonspherical NPs, these authors suggested the concept of an equivalent cylinder with the same translational and rotational diffusion coefficients as those of the real particle. This concept can be useful for monitoring the stability of NPs in liquid media and the changes in their size with time, which has been demonstrated using the example of gold nanorods subjected to selective etching.

The DDLS method was used to estimate the parameters of several suspensions of gold nanorods and a suspension of hematite ($Fe_2O_3$) rods, as well the changes in the size of gold nanorods upon selective etching [100]. For evaluating the DDLS data, all samples were also examined by TEM, and, for gold nanorods, the extinction spectra were measured in the spectral range around the localized surface plasmon resonance (LSPR) peak. The studies have shown that the method described in Ref. [100] can be used to calibrate nonspherical particles in liquid media. A study on citrate-coated gold nanorods [55] provides another example of the difference between the estimates of the nanorod sizes obtained by the DLS and DDLS methods.

Other structures, including tubes, disks, thin layers, ellipsoids of rotation, rings, hollow balls, and spherical shells with specified radius and thickness, have been considered [101]. Here, the DLS method could not be used in its classical form, because ensembles of NPs of irregular shape were studied. Therefore, the MADLS method was used for more accurate estimation of sizes. Equations have been derived for NPs of individual types, whose root-mean-square radii are defined, e.g. nanotubes (Eq. (17)), nanorods (Eq. (18)), nanolayers (Eq. (19)) and nanorings (Eq. (20)).

$$\langle r_g^2 \rangle = \frac{L}{12} + a^2 + \frac{t^2}{2} - at, \tag{17}$$

$$\langle r_g^2 \rangle = \frac{L^2}{12} + \frac{a^2}{2}, \tag{18}$$

$$\langle r_g^2 \rangle = \frac{1}{12}(L^2 + t^2 + \omega^2), \tag{19}$$

$$\langle r_g^2 \rangle = a^2 - at + \frac{7}{12}t^2, \tag{20}$$

where the nanotube has a length $L$, thickness $t$, and radius $a$; the uniform nanorod has a length $L$ and radius $a$; the nanolayer has a length $L$, width $w$, and thickness $t$; and the nanoring has an external radius $a$ and a square cross-section thickness $t$.

In conclusion, note that the DLS method in the classical form yields size estimates substantially differing from the actual ones when applied to asymmetrical particles.

Of no less interest are Janus particles, a subclass of anisotropic particles considered to be among the most complex colloidal particles available [102]. Janus particles have two sides with different surface features, structures, and compositions [103]. This asymmetric structure allows combining different and even incompatible physical, chemical, and mechanical properties within a single particle. A new class of Janus photonic particles based on poly(4-vinylpyridine)-r-polystyrene has been reported [104], capable of re-emitting light in a dynamically tunable range by varying the size of the particle and the molecular weights of dendronized block copolymers and poly(4-vinylpyridine)-r-polystyrene, as well as the mass ratio of these last two components. This material is promising for biomedical imaging. Much effort has been made to obtain Janus particles with a high homogeneity, tunable size and shape, combined functionalities, and scalable synthesis. An approach to the synthesis of such particles has been proposed [105]. Due to their unique properties, Janus particles have attracted attention in a wide range of applications, such as optics, catalysis, and biomedicine [102]. For example, several materials or combinations of materials can be incorporated into a single particle to provide controlled release of several drugs with independent release kinetics. This can be used to obtain synergistic effects of combination therapy and multilevel targeting that are impossible in the case of isotropic systems. Silicon-based Janus particles are known to be a promising material for biomedical imaging. In addition, anti-cancer effect of dual-loaded Janus particles against HeLa cells has been demonstrated, with doxorubicin (DOX) release monitored using the Förster energy transfer between DOX and 7-hydroxycoumarin-3-carboxylate [106]. Therefore, correct estimation of the size of Janus particles will allow the monitoring of drug release, and the estimation of the diffusion coefficient can be used to calculate the kinetics of Janus particle distribution in the human body. Onajite Shemi et al. [107] studied the behavior of spherical and elliptical Janus particles in water and in 8% hydrogen peroxide. The Janus spheres in hydrogen peroxide solution had a diffusion coefficient of $D = 0.60$ μm²s⁻¹ and an average velocity of $v = 1.9$ μm²s⁻¹. For comparison, 1.0-μm spherical Janus particles with a 5-nm platinum layer in 10% hydrogen peroxide had $D = 0.31$ μm²s⁻¹ and $v = 3.1$ μm²s⁻¹.

The DLS method has been used directly for estimating the Janus NP sizes [108]. Four types of polymeric NPs were synthesized: TCD1, TCD2, TCD3, and TCD4. TCD1 Janus NPs had a "snowman" morphology, and the other three types were spherical. According to the DLS data, the mean HR of TCD1 Janus NPs was 40 nm, which corresponded to the axial length of the "snowman"-like structure of TCD1 Janus NPs. The estimated mean HRs of TCD2, TCD3, and TCD4 NPs were 27.5, 34.5, and 79.5 nm, respectively.

Silicon Janus NPs doped with rhodamine and functionalized with 1,2-distearoyl-sn-glycero-3-phosphoethanolamine (DSPE) on one hemisphere of the

NP surface and a high-molecular-weight, long-chain poly(ethylene glycol) on another hemisphere were synthesized [109]. The size of the NPs as estimated by the DLS method was 50.5 ± 6 nm.

Because blood and water are similar in their physical characteristics, such experiments allow using DLS for qualitative estimation of the distribution of Janus NPs in the bloodstream, as well as their size, in order to implement flexible control of the release of the loaded drugs.

## *3.2 Measurement of Nanoparticle ζ-Potential*

In disperse systems, an electrical double layer (EDL) emerges on the surface of particles (at the particle–medium interface). EDL is a layer of ions formed on the particle surface as a result of adsorption of ions from solution or dissociation of surface compounds. The surface of the particle acquires a layer of ions of a certain sign evenly distributed over the surface and creating a charge on it. These ions are called potential-determining ions (PDIs). Ions of the opposite sign or counter-ions (CIs) are attracted to the particle surface from the liquid medium. Thus, the EDL consists of the PDI layer, and the CI layer located in the dispersion medium. The CI layer, in turn, also consists of two layers. The first layer is the adsorption layer (dense layer) adjacent to the interphase surface. This layer results from electrostatic interaction with PDIs and specific adsorption. The second layer is the diffusion layer, which contains CIs attracted to the particle due to electrostatic forces. The diffusion layer may be very thick, depending on the properties of the system.

When the particle moves, the EDL is disrupted. The place of disruption upon the movement of the solid and liquid phases relative to each other is called the slip plane. The slip plane lies at the boundary between the diffusion and adsorption layers, or in the diffusion layer near this boundary. The potential at the slip plane is called the electrokinetic potential or ζ-potential. It is calculated from the electrophoretic mobility of charged particles under the action of an applied electric field. The electrophoretic mobility of particles is equal to

$$U_p = \frac{V}{E}, \tag{21}$$

where $V$ is the speed of the particles (nm/s) and $E$ is the linear electric field intensity (V/cm).

The Helmholtz–Smoluchowski equation defines the relationship between the electrokinetic potential and the electrophoretic (electroosmotic) mobility:

$$\zeta \sim \frac{\eta \cdot U_p}{\varepsilon_r \varepsilon_0} = A \cdot \frac{\eta \cdot U_p}{\varepsilon_r \varepsilon_0}, \tag{22}$$

where $A$ is a coefficient depending on the size and concentration of the particles, η is the viscosity at the experimental temperature, $\varepsilon_r$ is the dielectric constant of the medium, and $\varepsilon_0$ is the electric constant (dielectric constant of the vacuum). More details on the calculation of the ζ-potential in practical applications are presented in Ref. [110].

The ζ-potential can be understood as the electric potential formed between the charged groups associated with the surface of the particle and the suspension medium. From the known value of ζ-potential, the surface charge of the particle can be deduced.

Laser Doppler velocimetry (LDV) uses the Doppler effect to measure the velocity of fluids or particles. LDVs have been used to estimate particle sizes [111]. However, the sizes of some NPs, such as micelles and liposomes [112], do not directly affect their velocities and, hence, cannot be directly measured using LDV. However, LDV can be used in conjunction with other techniques, such as DLS, to indirectly estimate the NP size from the velocity of NPs in a fluid. This information can then be used to correct the DLS measurements of the NP hydrodynamic diameter and obtain a more accurate estimation. The combination of the two methods has been used to measure the ζ-potentials of Ag, Cu, Ag/Cu [113], $Al_2O_3$, Al, HC-Ag, $SiO_2$, and $TiO_2$ NPs [114].

The DLS method can be used to determine the surface charges of lipid exosomes, polymeric microcapsules or particles, QDs, and other microparticles and NPs. For example, lysosomes are used as a biomarker of diseases, including Alzheimer's disease and cancer, estimation of the liposome surface charge being an essential diagnostic step [115]. Determination of the surface charge is a step in obtaining polymeric microcapsules whose shell consists of oppositely charged electrolytes. Such microcapsules can be used for encapsulation and targeted delivery of anticancer drugs [116], for biological imaging [117], and for engineering of multiplexed diagnostic systems based on suspension microarrays [118]. The fabrication of all these diverse nanosystems involves layer-by-layer deposition of oppositely charged electrolytes, fluorescent tags, and sometimes drugs, and precisely the electrostatic interaction between adjacent layers determines the assembly and stabilization of the layers.

Estimating the charge of microparticles and NPs is also important from a toxicological point of view. For example, the NP charge largely determines the mechanisms of NP entry into cells and their toxic effect. Specifically, positively charged NPs interact better with the negatively charged cell membrane or DNA and, hence, are more toxic than neutral or negatively charged NPs [58]. This tendency of microparticles and NPs of different charges to accumulate differently in different tissues is also used in designing delivery vehicles for anticancer drugs [119]. In addition, NPs can serve as centers of self-association or fibrillation of proteins and peptides, provoking amyloid-like proteinopathies, or, conversely, inhibitors of protein self-association. For example, Sukhanova et al. [120] have shown that only certain combinations of NP size and surface charge induce insulin fibrillation, and even minor changes in these parameters significantly reduce its rate.

Estimating the ζ-potential of QDs is an equally demanding task. QDs are characterized by a number of optical properties, including a high quantum yield, high brightness, high extinction coefficient, high resistance to photobleaching, as well as intermittent fluorescence signals (blinking), that have determined the wide use of QDs in medicine, particularly in medical imaging [121]. At the same time, QDs are potentially toxic, their characteristic size and the composition of their surface ligands and protein corona directly affecting the toxicity of QDs [122]. Nifontova et al. [123] used QDs as fluorescent nanolabels for hollow polyelectrolyte microcapsules. The microcapsules were assembled of several layers formed over calcium carbonate cores through successive precipitation from polystyrene sulfonate, peracetic acid, and polycyclic aromatic hydrocarbon solutions, and DLS estimation of the ζ-potential upon the formation of each layer is essential because it determines the success of the microcapsule synthesis. The size of the original calcium carbonate particles should be known for selecting the concentrations of the initial solutions used for layer-by-layer adsorption of polyelectrolyte polymers and the colloidal suspensions of hydrophilic magnetic NPs of iron (II, III) oxide with a carboxylated surface loaded into some microcapsules.

## *3.3 Designing Theranostic Agents for in Vitro/in Vivo Fluorescence Imaging, Magnetic Resonance Imaging, and Magnetically Controlled Drug Delivery and Release*

Correct estimation of QD sizes is necessary in some immunostaining techniques where antigen–antibody interaction is accompanied by the Förster resonance energy transfer from QDs to reference fluorophores. This approach is relevant if, e.g., CdSe/ZnS core/shell QDs surrounded with a specific protein corona are used to detect free tumor biomarkers, such as prostate-specific antigen (PSA), in human serum samples [124]. In a study on improving the aforementioned microcapsule technology, Nifontova et al. [117] reported the mean HRs and ζ-potentials of the main building blocks of the microcapsules measured by the DLS method. The sizes of different building blocks ranged from about 31 nm to about 4137 nm, and their ζ-potentials ranged from –41.8 mV for the smallest block to –8.86 mV for the largest one. These parameters affect the photoluminescence of polyelectrolyte microcapsules with opposite surface charges in multicomponent media and, hence, the possibility of using this platform as an imaging agent.

## *3.4 Estimation of the Molecular Weight of Polymers*

Molecular weight is one of the most important properties of a molecule. Comparison of the reference molecular weights of proteins or nucleic acids with experimentally determined values can provide useful information on, e.g., the oligomeric state of the biomolecules, their degradation, and interactions between binding partners. For example, estimation of the molecular weight for confirming the absence of aggregates is a mandatory step in the testing of antibodies used for therapy [125]. Molecular weight estimation is also a convenient test for detecting interactions between molecules. Two approaches can be used for molecular weight estimation by the DLS method. The first is based on the calibration of the instrument using particles with a known molecular weight, such as ovalbumin (44 kDa, HR = 2.98 nm), aldolase (158 kDa, HR = 4.98), and other proteins. The second approach is based on combining data on the sedimentation coefficient obtained using an analytical ultracentrifuge and the HR measured by the DLS method, using the Svedberg equation [126]:

$$M_\omega = \frac{6\pi\eta_0 R_h N_A s^0_{20,\omega}}{1-\bar{\nu}\rho_0}, \quad (23)$$

where $s^0_{20,\omega}$ is the sedimentation coefficient converted to standard conditions (in water at 20°C) , $\bar{\nu}$ is the partial specific volume of the molecule, $\eta_0$ is the viscosity of the solvent at the experimental temperature $T$(°C), $\rho_0$ is the density of the solvent at the given temperature $T$(°C), $N_A$ is the Avogadro number, and $R_h$ the universal gas constant. This approach is widely used for estimating the molecular weights of proteins and nucleic acids [127, 128].

Another example of molecular weight estimation by the DLS method is reported by Badasyan et al. [129]. In order to correctly evaluate the results, identical solutions of dendritic molecules and polycarbosilane were analyzed by the DLS method and gel filtration chromatography (GFC) under the same conditions. By heating the diluted solutions, the agglomerates were broken up to obtain a molecular dispersion, i.e., the solution of individual dendrimer molecules, where the molecule size could be measured by the DLS method. The obtained HR value was used to measure the molecular weight of the globular structure of the dendrimer using the equation:

$$M_w = V\rho N_A = \frac{4\pi D^3}{6}\rho N_A, \quad (24)$$

where $N_A$ is the Avogadro number, $D$ is the particle diameter, $V$ is hydrodynamic particle volume, and the density ρ = 1.54 g/ml is assumed as a calculated one. In conclusion, it has to be noted that the measurement of the molecular weight by the DLS method is used for solving routine tasks, most commonly for the detection of dimers or other aggregations of protein molecules.

## *3.5 Dynamic Light Scattering in Dealing with Biopolymers*

The most common examples of using the DLS method for studying biological molecules are studies on protein aggregation and assembly of nucleic acid complexes,

formation of protein–protein and protein–nucleic acid complexes, and interactions between proteins and small molecules. Complex formation is detected by measuring the HRs of microparticles and NPs in solutions. For example, Patel et al. [130] used DLS analysis to study the interaction between the nidogen-1 membrane protein and the laminin γ-1 extracellular matrix glycoprotein, which plays a key role in cell membrane formation. The DLS method makes it possible to promptly study the formation of this complex and its degradation by various chemical agents. DLS can also be used to determine the equilibrium and dissociation constants, as shown by Sharma et al. [131] in experiments on the interaction of the fibroblast growth factor with its receptor. Similarly, the DLS method allows quick and high-throughput screening of molecules inhibiting the interaction of two proteins [132]. Test systems for DLS detection of viruses have also been developed. For example, Driskell et al. [133] used conjugates of antibodies against the influenza virus with GNPs and detected the formation of aggregates by the DLS method. The detection limit of this technique was less than 100 $TCID_{50}$ per milliliter (tissue culture infectious doses ($TCID_{50}$) is the number of infectious virus particles required to infect 50% of a given cell culture).

It is known that single-stranded nucleic acid molecules, particularly RNA, tend to form various secondary structures, e.g., hairpins and pseudoknots. The formation of one or another structure is determined by the nucleotide sequence of RNA, which makes it possible to search for single-nucleotide substitutions in the RNA sequence by estimating its size using the DLS method [134]. In addition, complementary nucleic acid strands may form dimers, which can be used for detecting viral or other specific RNA sequences. Finally, in 2020 Gao et al. [135] proposed a DLS method for ultrasensitive detection of microRNA in the rolling circle replication reaction. Further development of this approach could provide a simple, inexpensive method of cancer diagnosis based on DLS detection of microRNAs.

Applications of DLS to the analysis of biological molecules and polymers are practically unlimited and depend only on the design of the experiment. The use of DLS is still one of the easiest and least expensive approaches to high-throughput analysis of the properties of biological molecules; therefore, its applications for diagnosis and study of molecular interactions are rapidly widening.

## 4 Conclusions

The examples presented in this review article clearly demonstrate that DLS analysis has a number of unique advantages over other analytical methods, notwithstanding some challenges in the experimental techniques and data processing. The DLS method estimates parameters indispensable for characterization of biological molecules, microparticles and NPs, such as HR, surface charge, and molecular weight. Unlike transmission, scanning, and atomic force microscopies, DLS analysis is performed in the liquid phase, which is a natural medium for biological molecules. Furthermore, the HRs of protein globules, microparticles, and NPs coated with components of biological fluids are more natural parameters than the physical sizes of denatured protein molecules or solid shells of particles. The range of research and applied tasks solved by the DLS method includes testing of protein- and antibody-based drugs for stability and aggregability; study of the interaction between receptors and their ligands (proteins, nucleic acids, and small biomolecules); fabrication of multilayer polymeric functional microcapsules stabilized by electrostatic interaction forces to be used for drug delivery and imaging of lesions; characterization of nanomaterials for biological research, medicine, and electrical engineering; development of diagnostic test systems; and many others. The DLS analysis is advantageous over other analytical techniques due to its higher technical availability, ease of performing, and high throughput. In contrast to many microscopy techniques, the DLS method can be used to study dynamic processes, which is extremely important for biological and medical research. At the same time, the DLS method has a number of limitations and difficulties related to the selection of experimental conditions, such as the concentration range of solutions and the types of solvents, as well as additional mathematical calculations if the analyzed objects are not spherical. The DLS method dovetails with other analytical techniques, such as GFC and various types of microscopy, supplementing the results and simplifying the analysis of large amounts of samples, and it is also suitable for the study of dynamic processes.

Thus, having considered the physical principles of DLS necessary for understanding the DLS method and planning experiments with proper account of its strengths and limitations, as well as the examples of the use of this approach for solving specific research and applied problems, we can conclude that DLS analysis is promising for a variety of research areas.

## Disclosures

The authors have no relevant financial interest in this article and no conflict of interest to disclose.

## Acknowledgments

The research was carried out with financial support of the Russian Science Foundation, grant no. 21-79-30048.

## References


1. K. Rebrosova, O. Samek, M. Kizovsky, S. Bernatova, V. Hola, and F. Ruzicka, "Raman Spectroscopy – A Novel Method for Identification and Characterization of Microbes on a Single-Cell Level in Clinical Settings," Frontiers in Cellular and Infection Microbiology 12, 866463 (2022).
2. M. A. Kouri, E. Spyratou, M. Karnachoriti, Dimitris Kalatzis, N. Danias, N. Arkadopoulos, I. Seimenis, Y. S. Raptis, A. G. Kontos, and E. P. Efstathopoulos, "Raman Spectroscopy: A Personalized Decision-Making Tool on Clinicians' Hands for In Situ Cancer Diagnosis and Surgery Guidance," Cancers 14(5), 1144 (2022).
3. M. H. Simonian, "Spectrophotometric Determination of Protein Concentration," Current Protocols in Toxicology 21(1), A.3G.1–A.3G.7 (2004).
4. A. M. García-Alegría, I. Anduro-Corona, C. J. Pérez-Martínez, M. A. G. Corella-Madueño, M. L. Rascón-Durán, and H. Astiazaran-Garcia, "Quantification of DNA through the NanoDrop Spectrophotometer: Methodological Validation Using Standard Reference Material and Sprague Dawley Rat and Human DNA," International Journal of Analytical Chemistry 2020, 8896738 (2020).
5. W. H. Brooks, W. C. Guida, and K. G. Daniel, "The Significance of Chirality in Drug Design and Development," Current Topics in Medicinal Chemistry 11(7), 760–770 (2011).
6. R. Ding, J. Ying, and Y. Zhao, "An electronic circular dichroism spectroscopy method for the quantification of L – and D – amino acids in enantiomeric mixtures," Royal Society Open Science 8(3), 201963 (2021).
7. H. S. Son, Y. S. Hong, W. M. Park, M. A. Yu, and C. H. Lee, "A Novel Approach for Estimating Sugar and Alcohol Concentrations in Wines Using Refractometer and Hydrometer," Journal of Food Science 74(2), C106– C111 (2009).
8. P. Y. Liu, L. K. Chin, W. Ser, H. F. Chen, C.-M. Hsieh, C.-H. Lee, K.-B. Sung, T. C. Ayi, P. H. Yap, B. Liedberg, K. Wang, T. Bourouina, and Y. Leprince-Wang, "Cell refractive index for cell biology and disease diagnosis: past, present and future," Lab on a Chip 16(4), 634–644 (2016).
9. U. Bulbake, S. Doppalapudi, N. Kommineni, and W. Khan, "Liposomal Formulations in Clinical Use: An Updated Review," Pharmaceutics 9(2), 12 (2017).
10. Y. Jia, Y. Jiang, Y. He, W. Zhang, J. Zou, K. T. Magar, H. Boucetta, C. Teng, and W. He, "Approved Nanomedicine against Diseases," Pharmaceutics 15(3) 774 (2023).
11. Y. Yao, Y. Zhou, L. Liu, Y. Xu, Q. Chen, Y. Wang, S. Wu, Y. Deng, J. Zang, and A. Shao, "Nanoparticle-Based Drug Delivery in Cancer Therapy and Its Role in Overcoming Drug Resistance," Frontiers in Molecular Biosciences 7, 193 (2020).
12. A. C. Anselmo, and S. Mitragotri, "Nanoparticles in the clinic: An update," Bioengineering & Translational Medicine 4(3), e10143 (2019).
13. R. Raliya, T. Singh Chadha, K. Haddad, and P. Biswas, "Perspective on Nanoparticle Technology for Biomedical Use," Current Pharmaceutical Design 22(17), 2481–2490 (2016).
14. J. J. Giner-Casares, M. Henriksen-Lacey, M. Coronado-Puchau, and L. M. Liz-Marzán, "Inorganic nanoparticles for biomedicine: where materials scientists meet medical research," Materials Today 19(1), 19–28 (2016).
15. H. Moosmüller, W. P. Arnott, "Particle Optics in the Rayleigh Regime," Journal of the Air & Waste Management Association 59(9), 1028–1031(2009).
16. J. Jeevanandam, A. Barhoum, Y. S. Chan, A. Dufresne, and M. K. Danquah, "Review on nanoparticles and nanostructured materials: history, sources, toxicity and regulations," Beilstein Journal of Nanotechnology 9(1), 1050–1074 (2018).
17. M. Kaszuba, M. T. Connah, "Protein and Nanoparticle Characterisation Using Light Scattering Techniques," Particle & Particle Systems Characterization 23(2), 193–196 (2006).
18. A. Wishard, B. C. Gibb, "Dynamic light scattering – an all-purpose guide for the supramolecular chemist," Supramolecular Chemistry 31(9), 608–615 (2019).
19. N. Damaschke, H. Nobach, N. Semidetnov, and C. Tropea, "Optical particle sizing in backscatter," Applied Optics 41(27), 5713–5727 (2002).
20. M. Kaszuba, D. McKnight, M. T. Connah, F. K. McNeil-Watson, and U. Nobbmann, "Measuring sub nanometre sizes using dynamic light scattering," Journal of Nanoparticle Research 10, 823–829 (2008).
21. A. Kurzhals, K. Wulf, V. Senz, T. Eickner, N. Grabow, and W. Schmidt, "Determination of Infusion Filter Efficiency applying Dynamic Light Scattering," Current Directions in Biomedical Engineering 8(2), 485–488 (2022).
22. J. K. G. Dhont, C. G. de Kruif, "Scattered light intensity cross correlation. I. Theory," The Journal of Chemical Physics 79(4), 1658–1663 (1983).
23. A. V. Malm, J. C. W. Corbett, "Improved Dynamic Light Scattering using an adaptive and statistically driven time resolved treatment of correlation data," Scientific Reports 9, 13519 (2019).
24. K. Hou, C. Wang, and X. Liu, "Study on Backward Scattering Characteristics of Submicron Particles," Optics and Photonics Journal 10(5), 79–87 (2020).
25. C. Wang, K. Kou, and J. Yan, "Frequency-shifted nano-particle sizing using laser self-mixing interferometry under linear current tuning," Laser Physics Letters 19(6), 066202 (2022).

26. J. Herbert, K. Bertling, T. Taimre, A. D. Rakić, and S. Wilson, "Microparticle discrimination using laser feedback interferometry," Optics Express 26(20), 25778–25792 (2018).
27. K. Zhu, H. Chen, S. Zhang, Z. Shi, Y. Wang, and Y. Tan, "Frequency-Shifted Optical Feedback Measurement Technologies Using a Solid-State Microchip Laser," Applied Sciences 9(1), 109 (2018).
28. M. Draijer, E. Hondebrink, T. van Leeuwen, and W. Steenbergen, "Review of laser speckle contrast techniques for visualizing tissue perfusion," Lasers in Medical Science 24, 639–651 (2009).
29. Q. Zhang, J. C. Gamekkanda, A. Pandit, W. Tang, C. Papageorgiou, C. Mitchell, Y. Yang, M. Schwaerzler, T. Oyetunde, R. D. Braatz, A. S. Myerson, and G. Barbastathis, "Extracting particle size distribution from laser speckle with a physics-enhanced autocorrelation-based estimator (PEACE)," Nature Communications 14, 1159 (2023).
30. M. Sadrara, M. Miri, "Scattering of electromagnetic waves by a cluster of charged spherical nanoparticles," Journal of the Optical Society of America B 33(12), 2552 (2016).
31. J. C. Dyre, "Rayleigh scattering revisited," Nature Materials 15(11), 1150–1151 (2016).
32. X. Yu, Y. Shi, T. Wang, and X. Sun, "Dust-Concentration Measurement Based on Mie Scattering of a Laser Beam," PLoS ONE 12(8), e0181575 (2017).
33. Z. Cao, L. Xu, and J. Ding, "Integral inversion to Fraunhofer diffraction for particle sizing," Applied Optics 48(25), 4842–4850 (2009).
34. J. Vargas-Ubera, J. F. Aguilar, and D. M. Gale, "Reconstruction of particle-size distributions from light-scattering patterns using three inversion methods," Applied Optics 46(1), 124–132 (2007).
35. C. M. Keck, R. H. Müller, "Size analysis of submicron particles by laser diffractometry - 90% of the published measurements are false," International Journal of Pharmaceutic 355(1-2), 150–163 (2008).
36. G. Brodie, "Energy Transfer from Electromagnetic Fields to Materials," Chapter 4 in Electromagnetic Fields and Waves, H. Yeap, and K. Hirasawa (Eds.), IntechOpen, Rijeka, (2019).
37. A. Rahimzadegan, R. Alaee, C. Rockstuhl, and R. W. Boyd, "Minimalist Mie Coefficient Model," Optics Express 28(11), 16511 (2020).
38. X. Li, L. Xie, and X. Zheng, "The Comparison between the Mie Theory and the Rayleigh Approximation to Calculate the EM Scattering by Partially Charged Sand," Journal of Quantitative Spectroscopy and Radiative Transfer 113(3), 251–258 (2012).
39. R. Gutiérrez-Cuevas, N. J. Moore, and M. A. Alonso, "Lorenz-Mie Scattering of Focused Light via Complex Focus Fields: An Analytic Treatment," Physical Review A 97(5), 053848 (2018).
40. L. André Ambrosio, "Symmetry relations in the generalized Lorenz–Mie theory for lossless negative refractive index media," Journal of Quantitative Spectroscopy and Radiative Transfer 180, 147–153 (2016).
41. D. J. Lockwood, Encyclopedia of Color Science and Technology, Springer, Heidelberg (2016).
42. Y. Yue, Y. Kan, H. Choi, A. Clearfield, and H. Liang, "Correlating hydrodynamic radii with that of two-dimensional nanoparticles," Applied Physics Letters 107(25), 253103 (2015).
43. J. Zmpitas, J. Gross, "Modified Stokes–Einstein Equation for Molecular Self-Diffusion Based on Entropy Scaling," Industrial & Engineering Chemistry Research 60(11), 4453–4459 (2021).
44. M. A. Islam, "Einstein – Smoluchowski Diffusion Equation: A Discussion," Physica Scripta 70(2–3), 120–125 (2004).
45. K. Ishii, T. Iwai, "Theoretical Analysis of Path-Length-Resolved Power Spectrum Measurement Using Low-Coherence Dynamic Light Scattering," Japanese Journal of Applied Physics 47(11), 8397–8401 (2008).
46. D. Ferreira, R. Bachelard, W. Guerin, R. Kaiser, and M. Fouché, "Connecting field and intensity correlations: The Siegert relation and how to test it," American Journal of Physics 88(10), 831–837 (2020).
47. G. Derkachov, D. Jakubczyk, K. Kolwas, K. Piekarski, Y. Shopa, and M. Woźniaket, "Dynamic Light Scattering Investigation of Single Levitated Micrometre-Sized Droplets Containing Spherical Nanoparticles," Measurement 158, 107681 (2020).
48. S. C. Buranay, M. A. Özarslan, and S. S. Falahhesar, "Numerical Solution of the Fredholm and Volterra Integral Equations by Using Modified Bernstein–Kantorovich Operators," Mathematics 9(11), 1193 (2021).
49. R. Xu, Particle Characterization: Light Scattering Methods, Springer, Dordrecht (2000).
50. M. M. Hoffmann, M. D. Too, M. Vogel, T. Gutmann, and G. Buntkowsky, "Breakdown of the Stokes–Einstein Equation for Solutions of Water in Oil Reverse Micelles," The Journal of Physical Chemistry B 124(41), 9115–9125 (2020).
51. A. J. Banchio, M. Heinen, P. Holmqvist, and G. Nägeleet, "Short- and Long-Time Diffusion and Dynamic Scaling in Suspensions of Charged Colloidal Particles," The Journal of Chemical Physics 148(13), 134902 (2018).
52. M. Wang, M. Heinen, and J. F. Brady, "Short-Time Diffusion in Concentrated Bidisperse Hard-Sphere Suspensions," The Journal of Chemical Physics 142(6), 064905 (2015).
53. A. M. Fiore, J. W. Swan, "Fast Stokesian Dynamics," Journal of Fluid Mechanics 878, 544–597 (2019).
54. M. Naiim, A. Boualem, C. Ferre, M. Jabloun, A. Jalochaa, and P. Ravier, "Multiangle Dynamic Light Scattering for the Improvement of Multimodal Particle Size Distribution Measurements," Soft Matter 11(1), 28–32 (2015).

55. C. Geers, L. Rodriguez-Lorenzo, D. A. Urban, C. Kinnear, A. Petri-Fink, and S. Balog, "A New Angle on Dynamic Depolarized Light Scattering: Number-Averaged Size Distribution of Nanoparticles in Focus," Nanoscale 8(34), 15813–15821 (2016).
56. A. D. Levin, E. A. Shmytkova, and B. N. Khlebtsov, "Multipolarization Dynamic Light Scattering of Nonspherical Nanoparticles in Solution," The Journal of Physical Chemistry C 121(5), 3070–3077 (2017).
57. M. Alexander, D. G. Dalgleish, "Dynamic Light Scattering Techniques and Their Applications in Food Science," Food Biophysics 1, 2–13 (2006).
58. A. Sukhanova, S. Bozrova, P. Sokolov, M. Berestovoy, A. Karaulov, and I. Nabiev, "Dependence of Nanoparticle Toxicity on Their Physical and Chemical Properties," Nanoscale Research Letters 13(1), 44 (2018).
59. I. de la Calle, M. Menta, M. Klein, and F. Séby, "Screening of TiO2 and Au Nanoparticles in Cosmetics and Determination of Elemental Impurities by Multiple Techniques (DLS, SP-ICP-MS, ICP-MS and ICP-OES)," Talanta 171, 291–306 (2017).
60. M. Y. Chan, Q. M. Dowling, S. J. Sivananthan, and R. M. Kramer, "Particle Sizing of Nanoparticle Adjuvant Formulations by Dynamic Light Scattering (DLS) and Nanoparticle Tracking Analysis (NTA)," in Vaccine Adjuvants. Methods and Protokols, C. B. Fox (Eds.), Humana Press, New York, 239–252 (2017).
61. S. Skoglund, E. Blomberg, I. O. Wallinder, I. Grillo, J. S. Pedersen, and L. M. Bergström, "A Novel Explanation for the Enhanced Colloidal Stability of Silver Nanoparticles in the Presence of an Oppositely Charged Surfactant," Physical Chemistry Chemical Physics 19(41), 28037–28043 (2017).
62. G. Almeida, O. J. Ashton, L. Goldoni, D, Maggioni, U. Petralanda, N. Mishra, Q. A. Akkerman, I. Infante, H. J. Snaith, and L. Manna, "The Phosphine Oxide Route toward Lead Halide Perovskite Nanocrystals," Journal of the American Chemical Society 140(44), 14878–14886 (2018).
63. S. T. Moerz, A. Kraegeloh, M. Chanana, and T. Kraus, "Formation Mechanism for Stable Hybrid Clusters of Proteins and Nanoparticles," ACS Nano 9(7), 6696–6705 (2015).
64. S. P. Yeap, A. L. Ahmad, B. S. Ooi, and J. Lim, "Electrosteric Stabilization and Its Role in Cooperative Magnetophoresis of Colloidal Magnetic Nanoparticles," Langmuir 28(42), 14878–14891 (2012).
65. J. K. Lim, D. C. J. Chieh, S. A. Jalak, P. Y. Toh, N. H. M. Yasin, B. W. Ng, and A. L. Ahmad, "Rapid Magnetophoretic Separation of Microalgae," Small 8(11), 1683–1692 (2012).
66. L. C. Gonçalves, A. B. Seabra, M. T. Pelegrino, D. R. de Araujo, J. S. Bernardes, and P. S. Haddad, "Superparamagnetic Iron Oxide Nanoparticles Dispersed in Pluronic F127 Hydrogel: Potential Uses in Topical Applications," RSC Advances 7(24), 14496–14503 (2017).
67. Y. Gu, M. Yoshikiyo, A. Namai, D. Bonvin, A. Martinez, R. Piñol, P. Téllez, N. J. O. Silva, F. Ahrentorp, C. Johansson, J. Marco-Brualla, R. Moreno-Loshuertos, P. Fernández-Silva, Y. Cui, S. Ohkoshi, and A. Millán, "Magnetic Hyperthermia with ε- Fe2O3 Nanoparticles," RSC Advances 10(48), 28786–28797 (2020).
68. N. Guarrotxena, O. García, and I. Quijada-Garrido, "Synthesis of Au@polymer Nanohybrids with Transited Core-Shell Morphology from Concentric to Eccentric Emoji-N or Janus Nanoparticles," Scientific Reports 8(1), 5721 (2018).
69. J. B. Vines, J.-H. Yoon, N.-E. Ryu, D.-J. Lim, and H. Park, "Gold Nanoparticles for Photothermal Cancer Therapy," Frontiers in Chemistry 7, 167 (2019).
70. R. E. Cavicchi, D. C. Meier, C. Presser, V. M. Prabhu, and S. Guha, "Single Laser Pulse Effects on Suspended-Au-Nanoparticle Size Distributions and Morphology," The Journal of Physical Chemistry C 117(20), 10866–10875 (2013).
71. T. Zheng, S. Bott, and Q. Huo, "Techniques for Accurate Sizing of Gold Nanoparticles Using Dynamic Light Scattering with Particular Application to Chemical and Biological Sensing Based on Aggregate Formation," ACS Applied Materials & Interfaces 8(33), 21585–21594 (2016).
72. R. Fathima, A. Mujeeb, "Nonlinear Optical Investigations of Laser Generated Gold, Silver and Gold-Silver Alloy Nanoparticles and Optical Limiting Applications," Journal of Alloys and Compounds 858, 157667 (2021).
73. Y. Zhang, Y. Chen, P. Westerhoff, K. Hristovski, and J. C Crittenden, "Stability of Commercial Metal Oxide Nanoparticles in Water," Water Research 42(8–9), 2204–2212 (2008).
74. S. Rajkumar, M. Prabaharan, "Theranostics Based on Iron Oxide and Gold Nanoparticles for Imaging- Guided Photothermal and Photodynamic Therapy of Cancer," Current Topics in Medicinal Chemistry 17(16), 1858–1871 (2017).
75. M. Lehmann, W. Tabaka, T. Möller, A. Oppermann, D. Wöll, D. Volodkin, S. Wellert, and R. von Klitzing, "DLS Setup for in Situ Measurements of Photoinduced Size Changes of Microgel-Based Hybrid Particles," Langmuir 34(12), 3597–3603 (2018).
76. Z. H. Chen, C. Kim, X. Zeng, S. H. Hwang, J. Jang, and G. Ungar, "Characterizing Size and Porosity of Hollow Nanoparticles: SAXS, SANS, TEM, DLS, and Adsorption Isotherms Compared," Langmuir 28(43), 15350–15361 (2012).
77. J. C. Wong, L. Xiang, K. H. Ngoi, C. H. Chia, K. S. Jin, and M. Ree, "Quantitative Structural Analysis of Polystyrene Nanoparticles Using Synchrotron X-Ray Scattering and Dynamic Light Scattering," Polymers 12(2), 477 (2020).

78. P. Eaton, P. Quaresma, C. Soares, C. Neves, M.P. de Almeida, E. Pereira, and P. West, "A direct Comparison of Experimental Methods to Measure Dimensions of Synthetic Nanoparticles," Ultramicroscopy 182, 179–190 (2017).
79. X. Liu, Q. Dai, L. Austin, J. Coutts, G. Knowles, J. Zou, H. Chen, and Q. Huo, "A One-Step Homogeneous Immunoassay for Cancer Biomarker Detection Using Gold Nanoparticle Probes Coupled with Dynamic Light Scattering," Journal of the American Chemical Society 130(9), 2780–2782 (2008).
80. Q. Dai, X. Liu, J. Coutts, L. Austin, and Q. Huo, "A One-Step Highly Sensitive Method for DNA Detection Using Dynamic Light Scattering," Journal of the American Chemical Society 130(26), 8138–8139 (2008).
81. C. T. Matea, T. Mocan, F. Tabaran, T. Pop, O. Mosteanu, C. Puia, C. Iancu and L. Mocan, "Quantum Dots in Imaging, Drug Delivery and Sensor Applications," International Journal of Nanomedicine 12, 5421–5431 (2017).
82. D. Geißler, C. Gollwitzer, A. Sikora, C. Minelli, M. Krumrey, and U. Resch-Genger, "Effect of fluorescent staining on size measurements of polymeric nanoparticles using DLS and SAXS," Analytical Methods 7(23), 9785–9790 (2015).
83. P. Modlitbová, K. Klepárník, Z. Farka, P. Pořízka, P. Skládal, K. Novotný, and J. Kaiser, "Time-Dependent Growth of Silica Shells on CdTe Quantum Dots," Nanomaterials 8(6), 439 (2018).
84. F. Cao, D. Yu, W. Ma, X. Xu, B. Cai, Y. M. Yang, S. Liu, L. He, Y. Ke, S. Lan, K.-L. Choy, and H. Zeng, "Shining Emitter in a Stable Host: Design of Halide Perovskite Scintillators for X-Ray Imaging from Commercial Concept," ACS Nano 14(5), 5183–5193 (2020).
85. J. Leinonen, S. Kneifel, and R. J. Hogan, "Evaluation of the Rayleigh–Gans Approximation for Microwave Scattering by Rimed Snowflakes," Quarterly Journal of the Royal Meteorological Society 144(S1), 77–88 (2018).
86. B. Ankamwar, "Size and Shape Effect on Biomedical Applications of Nanomaterials," Chapter 4 in Biomedical Engineering – Technical Applications in Medicine, R. Hudak (Ed.), InTechOpen, Rijeka (2012).
87. Y. Chen, Z. Fan, Z. Zhang, W. Niu, C. Li, N. Yang, B. Chen, and H. Zhang, "Two-Dimensional Metal Nanomaterials: Synthesis, Properties, and Applications," Chemical Reviews 118(13), 6409–6455 (2018).
88. J. Yang, Z. Zeng, J. Kang, S. Betzler, C. Czarnik, X. Zhang, C. Ophus, C. Yu, K. Bustillo, M. Pan, J. Qiu, L.-W. Wang, and H. Zheng, "Formation of Two-Dimensional Transition Metal Oxide Nanosheets with Nanoparticles as Intermediates," Nature Materials 18(9), 970–976 (2019).
89. H. Zhao, X. Chen, G. Wang, Y. Qiu, and L. Guo, "Two-Dimensional Amorphous Nanomaterials: Synthesis and Applications," 2D Materials 6(3), 032002 (2019).
90. F. Yang, P. Song, M. Ruan, and W. Xu, "Recent Progress in Two-Dimensional Nanomaterials: Synthesis, Engineering, and Applications," FlatChem 18, 100133 (2019).
91. Z. Liu, H. Chen, Y. Jia, W. Zhang, H. Zhao, W. Fan, W. Zhang, H. Zhong, Y. Nia, and Z. Guo, "A Two-Dimensional Fingerprint Nanoprobe Based on Black Phosphorus for Bio-SERS Analysis and Chemo-Photothermal Therapy," Nanoscale 10(39), 18795–18804 (2018).
92. Z. Xie, D. Wang, T. Fan, C. Xing, Z. Li, W. Tao, L. Liu, S. Bao, D. Fan, and H. Zhang, "Black phosphorus Analogue Tin Sulfide Nanosheets: Synthesis and Application as near-Infrared Photothermal Agents and Drug Delivery Platforms for Cancer Therapy," Journal of Materials Chemistry B 6(29), 4747–4755 (2018).
93. H. Zhang, T. Fan, W. Chen, Y. Li, and B. Wang, "Recent Advances of Two-Dimensional Materials in Smart Drug Delivery Nano-Systems," Bioactive Materials 5(4), 1071–1086 (2020).
94. J. A. Mariano-Torres, A. López-Marure, M. García-Hernández, G. Basurto-Islas, and M. Á. Domínguez-Sánchez, "Synthesis and characterization of glycerol citrate polymer and yttrium oxide nanoparticles as a potential antibacterial material," Materials Transactions 59(12), 1915–1919 (2018).
95. M. Lotya, A. Rakovich, J. F. Donegan, and J. N. Coleman, "Measuring the Lateral Size of Liquid-Exfoliated Nanosheets with Dynamic Light Scattering," Nanotechnology 24(26), 265703 (2013).
96. C. A. Little, C. Batchelor-McAuley, N. P. Young, and R. G. Compton, "Shape and Size of Non-Spherical Silver Nanoparticles: Implications for Calculating Nanoparticle Number Concentrations," Nanoscale 10(34), 15943–15947 (2018).
97. O. I. Sukharevsky, G. S. Zalevsky, "3-D Electromagnetic Scattering by Ellipsoidal Silver Nanoparticles in Optical Band," In 2018 IEEE 17th International Conference on Mathematical Methods in Electromagnetic Theory (MMET), Kyiv, UKraine, 152–155 (2018).
98. F. Gao, L. Bai, S. Liu, R. Zhang, J. Zhang, X. Feng, Y. Zheng, and Y. Zhao, "Rationally Encapsulated Gold Nanorods Improving Both Linear and Nonlinear Photoacoustic Imaging Contrast in Vivo," Nanoscale 9(1), 79–86 (2017).
99. S. Liao, W. Yue, S. Cai, Q. Tang, W. Lu, L. Huang, T. Qi, and J. Liao, "Improvement of Gold Nanorods in Photothermal Therapy: Recent Progress and Perspective," Frontiers in Pharmacology 12, 664123 (2021).
100. A. D. Levin, E. A. Shmytkova, "Nonspherical Nanoparticles Characterization by Partially Depolarized Dynamic Light Scattering," Proceedings of SPIE 9526, 95260P (2015).
101. P. J. Wyatt, "Measurement of Special Nanoparticle Structures by Light Scattering," Analytical Chemistry 86(15), 7171–7183 (2014).
102. H. Su, C.-A. H. Price, L. Jing, Q. Tian, J. Liu, and K. Qian, "Janus Particles: Design, Preparation, and Biomedical Applications," Materials Today Bio 4, 100033 (2019).

103. G. Agrawal, R. Agrawal, "Janus Nanoparticles: Recent Advances in Their Interfacial and Biomedical Applications," ACS Applied Nano Materials 2(4), 1738–1757 (2019).
104. Q. He, H. Vijayamohanan, J. Li, and T. M. Swager, "Multifunctional Photonic Janus Particles," Journal of the American Chemical Society 144(12), 5661–5667 (2022).
105. J. Wang, X. Chen, F. Lang, L. Yang, D. Qiu, and Z. Yang, "Large Scale Synthesis of Single-Chain/Colloid Janus Nanoparticles with Tunable Composition," Chemical Communications 56(27), 3875–3878 (2020).
106. H. Cao, Y. Yang, X. Chen, and Z. Shao, "Intelligent Janus nanoparticles for intracellular real-time monitoring of dual drug release," Nanoscale 8, 6754–6760 (2016).
107. O. Shemi, M. J. Solomon, "Self-Propulsion and Active Motion of Janus Ellipsoids," The Journal of Physical Chemistry B 122(44), 10247–10255 (2018).
108. W. Zhang, J. He, and X. Dong, "Controlled Fabrication of Polymeric Janus Nanoparticles and Their Solution Behaviors," RSC Advances 6(107), 105070–105075 (2016).
109. R. Kadam, J. Ghawali, M. Waespy, M. Maas, and K. Rezwan, "Janus Nanoparticles Designed for Extended Cell Surface Attachment," Nanoscale 12(36), 18938–18949 (2020).
110. S. Bhattacharjee, "DLS and Zeta Potential – What They Are and What They Are Not?" Journal of Controlled Release 235, 337–351 (2016).
111. J. C. Wilson, B. Y. H. Liu, "Aerodynamic particle size measurement by laser-doppler velocimetry," Journal of Aerosol Science 11(2), 139–150 (1980).
112. S. Dattani, X. Li, C. Lampa, D. Lechuga-Ballesteros, A. Barriscale, B. Damadzadeh, and B. R. Jasti, "A comparative study on micelles, liposomes and solid lipid nanoparticles for paclitaxel delivery," International Journal of Pharmaceutics 631, 122464 (2023).
113. D. Gonzalez-Mendoza, B. Valdez-Salas, E. Bernardo-Mazariegos, O. Tzintzun-Camacho, F. Gutiérrez-Miceli, V. Ruíz-Valdiviezo, L. Rodríguez-Hernández, and G. Sanchez-Viveros, "Influence of monometallic and bimetallic phytonanoparticles on physiological status of mezquite," Open Life Sciences 14(1), 62–68 (2019).
114. R. C. Murdock, L. Braydich-Stolle, A. M. Schrand, J. J. Schlager, and S. M. Hussain, "Characterization of Nanomaterial Dispersion in Solution Prior to In Vitro Exposure Using Dynamic Light Scattering Technique," Toxicological Sciences 101(2), 239–253 (2008).
115. M. K. Rasmussen, J. N. Pedersen, and R. Marie, "Size and Surface Charge Characterization of Nanoparticles with a Salt Gradient," Nature Communications 11(1), 2337 (2020).
116. G. Nifontova, T. Tsoi, A. Karaulov, I. Nabiev, and A. Sukhanova, "Structure–Function Relationships in Polymeric Multilayer Capsules Designed for Cancer Drug Delivery," Biomaterials Science 10(18), 5092–5115 (2022).
117. G. Nifontova, V. Krivenkov, M. Zvaigzne, A. Efimov, E. Korostylev, S. Zarubin, A. Karaulov, I. Nabiev, and A. Sukhanova, "Nanoparticle-Doped Hybrid Polyelectrolyte Microcapsules with Controlled Photoluminescence for Potential Bioimaging Applications," Polymers 13(23), 4076 (2021).
118. R. Bilan, A. Ametzazurra, K. Brazhnik, S. Escorza, D. Fernández, M. Uríbarri, I. Nabiev, and A. Sukhanova, "Quantum-Dot-Based Suspension Microarray for Multiplex Detection of Lung Cancer Markers: Preclinical Validation and Comparison with the Luminex XMAP® System," Scientific Reports 7(1), 44668 (2017).
119. H.-X. Wang, Z.-Q. Zuo, J.-Z. Du, Y.-C. Wang, R. Sun, Z.-T. Cao, X.-D. Ye, J.-L. Wang, K. W. Leong, and J. Wang, "Surface Charge Critically Affects Tumor Penetration and Therapeutic Efficacy of Cancer Nanomedicines," Nano Today 11(2), 133–144 (2016).
120. A. Sukhanova, S. Poly, S. Bozrova, É. Lambert, M. Ewald, A. Karaulov, M. Molinari, and I. Nabiev, "Nanoparticles With a Specific Size and Surface Charge Promote Disruption of the Secondary Structure and Amyloid-Like Fibrillation of Human Insulin Under Physiological Conditions," Frontiers in Chemistry 7, 480 (2019).
121. A. A. Abdellatif, M. A. Younis, M. Alsharidah, O. A. Rugaie, and H. M. Tawfeek, "Biomedical Applications of Quantum Dots: Overview, Challenges, and Clinical Potential," International Journal of Nanomedicine 17, 1951–1970 (2022).
122. 1A. Sukhanova, S. Bozrova, E. Gerasimovich, M. Baryshnikova, Z. Sokolova, P. Samokhvalov, C. Guhrenz, N. Gaponik, A. Karaulov, and I. Nabiev, "Dependence of Quantum Dot Toxicity In Vitro on Their Size, Chemical Composition, and Surface Charge," Nanomaterials 12(16), 2734 (2022).
123. G. Nifontova, F. Ramos-Gomes, F. Alves, I. Nabiev, and A. Sukhanova, "Stimulus-Sensitive Theranostic Delivery Systems Based on Microcapsules Encoded with Quantum Dots and Magnetic Nanoparticles," in Quantum Dots: Applications in Biology, A. Fontes, B. Santos (Eds.), Humana, New York, 199–212 (2020).
124. T. Tsoy, A. Karaulov, I. Nabiev, and A. Sukhanova, "Multiplexed Detection of Cancer Serum Antigens with a Quantum Dot-Based Lab-on-Bead System," in Quantum Dots: Applications in Biology, A. Fontes, B. Santos (Eds.), Humana, New York, 225–236 (2020).
125. C. G. Conner, J. McAndrew, S. Menegatti, and O. D. Velev, "An Accelerated Antibody Aggregation Test Based on Time Sequenced Dynamic Light Scattering," Colloids and Surfaces A: Physicochemical and Engineering Aspects 653, 129833 (2022).
126. W. A. Lindner, J. M. Brand, "A Coherent Approach to the Svedberg Equation," Biochemical Education 15(2), 71–72 (1987).

127. E. Dzananovic, T. R. Patel, G. Chojnowski, M. J. Boniecki, S. Deo, K. McEleney, S. E. Harding, J. M. Bujnicki, and S. A. McKenna, "Solution Conformation of Adenovirus Virus Associated RNA-I and Its Interaction with PKR," Journal of Structural Biology 185(1), 48–57 (2014).
128. T. R. Patel, M. Meier, J. Li, G. Morris, A. J. Rowe, and J. Stetefeld, "T-shaped Arrangement of the Recombinant Agrin G3 - IgG Fc Protein," Protein Science 20(6), 931–940 (2011).
129. A. Badasyan, A. Mavrič, I. K. Cigić, T. Bencik, and M. Valant, "Polymer Nanoparticle Sizes from Dynamic Light Scattering and Size Exclusion Chromatography: The Case Study of Polysilanes," Soft Matter 14(23), 4735–4740 (2018).
130. T. R. Patel, C. Bernards, M. Meier, K. McEleney, D. J. Winzor, M. Koch, and J. Stetefeld, "Structural Elucidation of Full-Length Nidogen and the Laminin–Nidogen Complex in Solution," Matrix Biology 33, 60–67 (2014).
131. P. Sharma, D. Rajalingam, T. K. S. Kumar, and S. Singh, "A Light Scattering Study of the Interaction of Fibroblast Growth Factor (FGF) with Its Receptor," Biophysical Journal 94(9), L71–L73 (2008).
132. A. D. Hanlon, M. I. Larkin, and R. M. Reddick, "Free-Solution, Label-Free Protein-Protein Interactions Characterized by Dynamic Light Scattering," Biophysical Journal 98(2), 297–304 (2010).
133. J. D. Driskell, C. A. Jones, S. M. Tompkins, and R. A. Tripp, "One-Step Assay for Detecting Influenza Virus Using Dynamic Light Scattering and Gold Nanoparticles," The Analyst 136(15), 3083 (2011).
134. E. Dzananovic, Astha, G. Chojnowski, S. Deo, E. P. Booy, P. Padilla-Meier, K. McEleney, J. M. Bujnicki, T. R. Patel, and S. A. McKenna, "Impact of the Structural Integrity of the Three-Way Junction of Adenovirus VAI RNA on PKR Inhibition," PLoS ONE 12(10), e0186849 (2017).
135. Y. Gao, S. Xu, T. He, J. Li, L. Liu, Y. Zhang, S. Ge, M. Yan, H. Liu, and J. Yu, "Ultrasensitive and Specific MicroRNA Detection via Dynamic Light Scattering of DNA Network Based on Rolling Circle Amplification," Sensors and Actuators B: Chemical 324, 128693 (2020).